Thermal Surge in Diffusion Welding—Generation, Inrush Characteristic and Effects

Heating separate members to different temperatures during the DFW process causes dynamic changes in the heat flux and creates the possibility of influencing the microstructure of the joint

BY J. GODZIEMBA-MALISZEWSKI

ABSTRACT. The diffusion welding process (DFW) has, till now, been very thermally stable in comparison with other welding processes. This stability and the favorable economic aspects of DFW are the reasons that methods for process acceleration and diffusion zone formation have been sought. In the present report, a new heating procedure in DFW process is described. In this procedure, termed DFW/TS, the heating of separate members to different temperatures creates, after pressing, a thermal surge in the colder member. Consequently, in the boundary layer of the joint, a thermal spike, a large thermal gradient and heat flux, comes into existence and leads to a sudden increase in the temperature of the colder part. It creates the possibilities of influencing the joint microstructure and the range of plastic deformation.

A simple mathematical model is presented to characterize the thermal surge and evaluate variations of the temperature, thermal spike, thermal gradient and heat flux density at the distance function from surface of contact and in the time function after pressing. The application of these equations to standard welds was required to execute simplifications and approximations. This has made it possible to estimate the data necessary for inrush characteristics and to calculate the variables of DFW/TS. For the example of iron-titanium diffusion welding, the method of measuring temperature, thermal gradient, and heat flux density is presented. The difference in microstructure and microhardness of the diffusion zone is demonstrated by a comparison of the Fe-Ti joints, which have been welded by DFW/TS and conventional DFW.

It was found that the new procedure of heating gives possibilities of controlling thermal energy flow through the contacted surfaces. The temperatures of the members and selection of the member to be heated to the higher temperature have an essential influence on the dynamics of the thermal effects, and thereby, on the joint structure.

J. GODZIEMBA-MALISZEWSKI is a Scientist and Teacher at the Technical University of Warsaw, Poland, now working as a Guest Scientist at the Jülich Nuclear Centre, FRG.

Introduction

Modern welding technologies use heat sources which possess a relatively large power output, considerable concentration of thermal flux and the fine control of the heat energy quantity, an essential to joining. For example, in Fig. 1, the electron beam unit (2) can generate concentrated power with a maximum density of 10^6 to 10^8 kW/m^2. The power of the heat source can be controlled in the range of 1 W to 50 kW, and the diameter of the weld pool is not large, ranging from $3 \cdot 10^{-3}$ to $2 \cdot 10^{-5}$ m. The equipment for laser beam welding (1), arc welding (3), and electroslag welding (4), in comparison with oxyacetylene welding (5), can be determined from Ref. 1. Apart from the influence on the microstructure of the joints by the thermal regime, a number of welding processes have possibilities of producing metallurgical effects in the weld metal.

KEY WORDS

Diffusion Welding
Thermal Surge
Process Acceleration
Separate Members
Dynamic Heat Flow
Thermal Spike
Thermal Diffusion
Oxide Films
Intermetallics
Fe-Ti DFW Joints

As opposed to the above examples, diffusion welding equipment creates very stable thermal conditions without any significant concentration of heat in a boundary layer of the joint. Radiator elements or heating inductors of high frequency are usually employed as thermal sources. Those heating systems can have considerable power with a fine control of the heat energy quantity. By the application of such heating systems, it is impossible in conventional DFW to get a concentration of heat flux in the boundary layer of a diffusion welded joint. It is also impossible to influence the joint's microstructure and to minimize the material's volume heating to high temperature. Therefore, it is generally accepted that diffusion welding is suited for the joining of similar or dissimilar metals which are particularly difficult to join by conventional techniques. However, the factors which have a negative effect on the strength of such joints have already been reported in the literature. Oxide films and intermetallic compounds are of great importance in this matter. Usually very stable and difficult to dissolve, oxide film on the faying surfaces is regarded as one of the most important factors which makes contact between metallic surfaces difficult and which prevents the formation of a metallic fusion between the faying surfaces (Ref. 2). In the second place, a lot of metal combinations form brittle intermetallic compounds in a fusion zone (Ref. 3). The long duration of a DFW process (Fig. 2) and the slow diffusion are conducive to the creation of intermetallic layers (Ref. 4).

Several studies on the prevention of such precipitate formation have been performed, leading to numerous variations of DFW. A few of them are: superplastic forming (SPF/DB) (Ref. 5), hot isostatic pressure (HIP) (Ref. 6), electro-

static field formed around the pieces to be welded (Ref. 7), flow of the current pulses through the faying surfaces (Ref. 8), torsional vibrations in the planes of the joints (or friction welding in vacuum) causing scuffing (Ref. 9), ultrasonic activation (Ref. 10), constant temperature gradient (Refs. 11, 12) and interlayer metal.

The aim of these DFW variations is to shorten the welding duration of the process. It is realized that the surface oxide films can be crushed and dissolved by accelerating the metallic contact over the largest possible surface and by intensifying the mass transport during the diffusion process. Many well-known DFW variations have defects, the most glaring being expense and limited applications.

The present report describes a new procedure (DFW/TS) of diffusion welding consisting of heating separate members to different temperatures, with the aim of getting thermal surge after pressing (Ref. 13)—Fig. 3. As a result, in the boundary layer of the colder part, a rapid, momentary increase in temperature has taken place, referred to as the thermal spike. The profile of the change in temperature has an influence on thermal gradient value and thermal flux density. Thermal flux flowing through contacted surfaces causes a thermal mass transport known as thermodiffusion (Soret effect). A rapid, momentary increase in temperature in the thin surface layer of the colder part, along with suitable welding variables, can lead to a melting of this layer. This is advantageous in joining metals which are covered by a thin oxide film (Ref. 21). The results indicate that the new heating procedure is simple to apply, shortens the process time, and furthermore, creates extensive possibilities for influencing the structure of the weld zone.

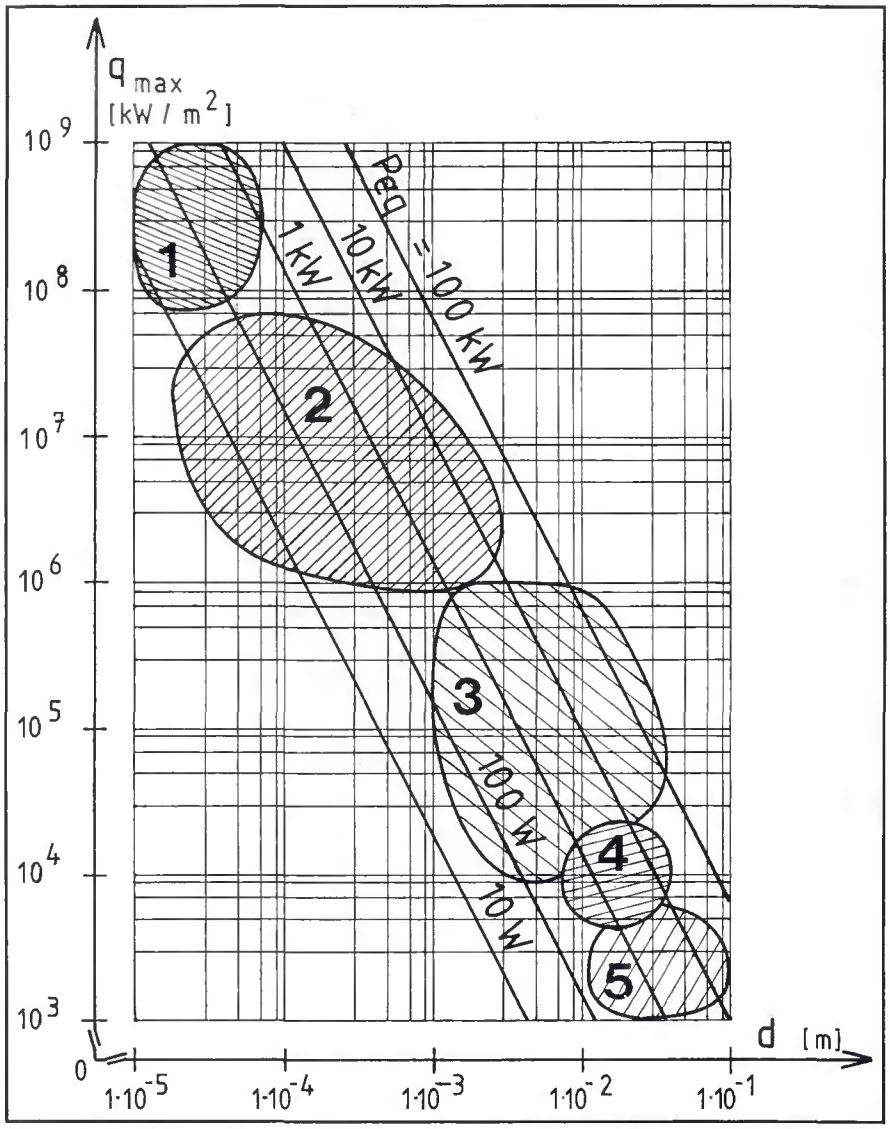

Fig. 1—Comparison of the constant in time, maximal heat flux density (q_{max}) obtained in fusion welding processes performed with selected welding equipment, such as: laser beam (1), electron beam (2), transferred arc (especially submerged arc welding) (3), electroslag (4), and oxyacetylene flame (5). (The heat losses are neglected.) The values are presented according to the power output of the welding equipment (P_{eq}) and according to the diameter of the weld pool (d) (Ref. 1)

Experimental Procedure

Assumption of the Evaluation

To characterize the thermal effects occurring in the boundary layer of the colder part after pressing the members together, it is necessary to know the temperature distribution in the thermal field as a function of time and distance from surface contact. From this relation, it is possible to determine the thermal gradient and heat flux density functions.

The values mentioned above, symptomatic of variability in the thermal field, are related to each other and allow thermal effects in the joint to be characterized. These values resulted from the behavior of the heat source, the control range of power, and the physical properties of the joined metals, all of which have great influence on the structure and qualities of the joint. The possibility of measuring or calculating these values creates conditions which establish their influence on the structure of the joint and leads to the optimization of production.

During joining by DFW/TS process, the flow of heat across the contacted surfaces of both parts has dynamic variable values and lasts but a very short time through the thin boundary layer of both metals. For these reasons, the characterization of the thermal effects in joints by measurements of the relevant physical quantity is very difficult. In order to characterize these effects, it was necessary to perform calculations on the basis of the simplified mathematical model. The unlimited bar in the y-axis position, composed of two parts, is described by inequalities $y_1 \leq 0$ and $y_2 \geq 0$—Fig. 4A. For each part, suitable thermal conductivities λ_1, λ_2; specific heats c_{p1}, c_{p2}; and specific gravities g_1, g_2 are attributed to both metals. Before contact, in the initial instant $t = 0$, the temperature of both parts T_1' and T_2' is constant, and $T_1' > T_2'$. At the moment $t > 0$, that is, after contact (Fig. 4B), the temperatures of both connected surfaces are equal, and the contact temperature T_c is constant in time. However, the heat losses by evaporation and thermal conduction are neglected, and the quantity of the heat flow across the contacted surfaces of the joint is constant in time.

The search distributions of the temperature $T_1(y_1,t)$, $T_2(y_2,t)$ and thermal gradients $\frac{T_1}{y_1}(y_1,t)$, $\frac{T_2}{y_2}(y_2,t)$ as functions of distances y_1 and y_2 from the contact place 0 of both parts of the bar at the moment $t > 0$ are the aim of the calcula-

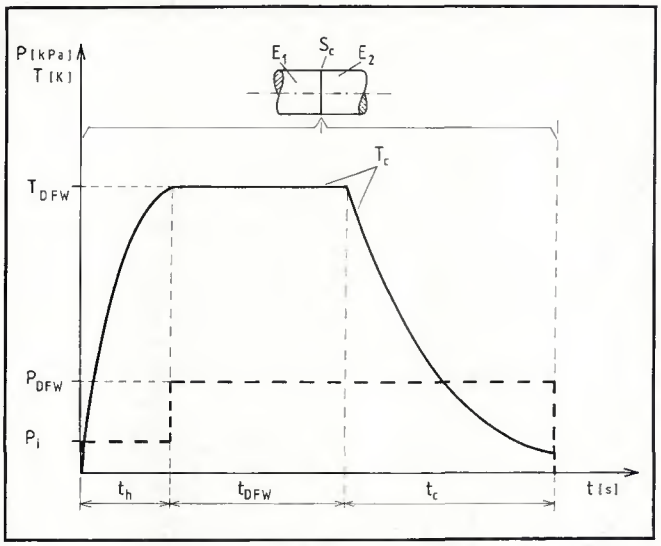

Fig. 2 – The course of temperature changes in the conventional diffusion welding (DFW) procedure: E_1 and E_2, elements to be welded are in contact with each other for the whole time of heating (t_h); welding t_{DFW} and cooling t_c; T_{DFW}, temperature of DFW process; T_c, contact temperature of two elements during heating, welding and cooling; P_i, initial pressure of elements; P_{DFW}, welding pressure of elements during DFW and cooling; S_c, contact surface of both elements

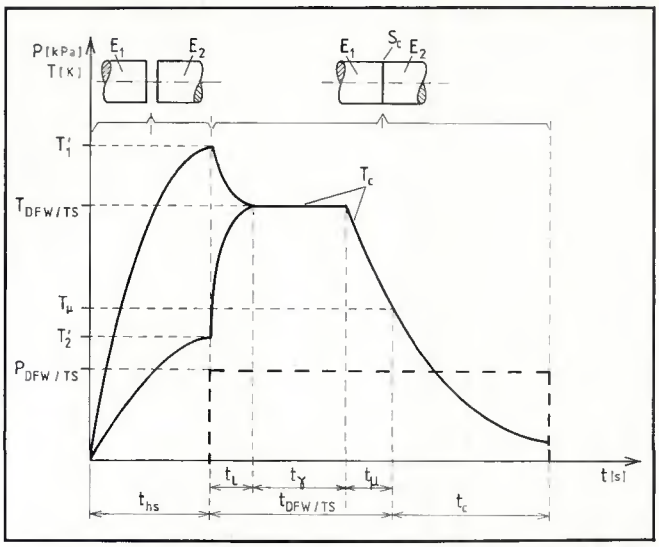

Fig. 3 – The course of temperature changes in DFW/TS during the heating of the separate elements to different temperatures t_{hs}, welding $t_{DFW/TS}$ and cooling t_c; T'_1 and T'_2, temperatures of elements E_1 and E_2 separated from each other in the heating time t_{hs}; $T_{DFW/TS}$, temperature of DFW/TS in the time $t_{DFW/TS}$; T_c, temperature of surfaces of both elements during welding $t_{DFW/TS}$ and cooling t_c to the end temperature T_μ of the diffusion process; $P_{DFW/TS}$, welding pressure of elements; S_c, contact surface of both elements

tion. The required temperatures satisfy the differential equations of heat conduction:

$$\alpha_1 \frac{\partial^2 T_1(y_1,t)}{\partial y_1^2} = \frac{\partial T_1(y_1,t)}{\partial t} \qquad (1')$$

$$\alpha_2 \frac{\partial^2 T_2(y_2,t)}{\partial y_2^2} = \frac{\partial T_2(y_2,t)}{\partial t} \qquad (1'')$$

and initial conditions:

$$T_1(y_1,0) = T'_1 \qquad (2')$$

$$T_2(y_2,0) = T'_2 \qquad (2'')$$

also boundary conditions:

$$T_1(0^-,t) = T_2(0^+,t) \qquad (3')$$

$$\lambda_1 \frac{\partial T_1(0^-,t)}{\partial y_1} = \lambda_2 \frac{\partial T_2(0^+,t)}{\partial y_2} \qquad (3'')$$

where:

$$\alpha_1 = \frac{\lambda_1}{c_{p1}\, g_1} \qquad (4')$$

$$\alpha_2 = \frac{\lambda_2}{c_{p2}\, g_2} \qquad (4'')$$

The required temperatures T_1, T_2 can be represented as a sum of constant functions and of the first kinds of thermal potentials:

$$T_1(y_1,t) = T'_1 + \frac{1}{2\sqrt{\pi}} \int_0^t \frac{\Theta_1(\tau)}{(t-\tau)^2} \exp\left[-\frac{y_1^2}{4\,\alpha_1(t-\tau)}\right] d\tau \qquad (5')$$

$$T_2(y_2,t) = T'_2 + \frac{1}{2\sqrt{\pi}} \int_0^t \frac{\Theta_2(\tau)}{(t-\tau)^2} \exp\left[-\frac{y_2^2}{4\,\alpha_2(t-\tau)}\right] d\tau \qquad (5'')$$

where: $\Theta_1(\tau)$, $\Theta_2(\tau)$ are any continuous functions for $t > 0$

The functions (Equations 5) satisfy the differential equations of heat conduction (Equations 1) and initial conditions (Equations 2).

The fulfillment of the boundary conditions (Equations 3) results in the system of integral equations and functional equations with unknowns $\Theta_1(\tau)$ and $\Theta_2(\tau)$:

$$\frac{1}{2\sqrt{\pi}}\int_0^t \frac{\Theta_2(\tau)-\Theta_1(\tau)}{\sqrt{t-\tau}}\,d\tau = T_1' - T_2' \tag{6'}$$

$$\frac{\lambda_1}{\sqrt{\alpha_1}}\Theta_1(\tau) + \frac{\lambda_2}{\sqrt{\alpha_2}}\Theta_2(\tau) = 0 \tag{6''}$$

where: $t > 0$

The solution of Equations 6 is a function of:

$$\Theta_1(\tau) = -\frac{2\lambda_2\sqrt{\alpha_1}}{\sqrt{\pi}(\lambda_1\sqrt{\alpha_2}+\lambda_2\sqrt{\alpha_1})}(T_1' - T_2')\frac{1}{\sqrt{t}} \tag{7'}$$

$$\Theta_2(\tau) = \frac{2\lambda_1\sqrt{\alpha_2}}{\sqrt{\pi}(\lambda_1\sqrt{\alpha_2}+\lambda_2\sqrt{\alpha_1})}(T_1' - T_2')\frac{1}{\sqrt{t}} \tag{7''}$$

Equations 7 and 5 yield:

$$T_1(y_1,t) = T_1' - \frac{T_1' - T_2'}{\pi} M_1 \int_0^t \frac{1}{\sqrt{t}\sqrt{t-\tau}} \exp\left[-\frac{y_1^2}{4\alpha_1(t-\tau)}\right] d\tau \tag{8'}$$

$$T_2(y_2,t) = T_2' + \frac{T_1' - T_2'}{\pi} M_2 \int_0^t \frac{1}{\sqrt{\tau}\sqrt{t-\tau}} \exp\left[-\frac{y_2^2}{4\alpha_2(t-\tau)}\right] d\tau \tag{8''}$$

Equations 8 give the temperature $T_1(y_1,t)$ and $T_2(y_2,t)$ as a function of the time and distance from the contacted surfaces. The analysis given above is valid if $y_1 < 0$, $y_2 > 0$ and $t > 0$. M_1 and M_2 were named the transfer coefficients and, as well as the dimensionless quantity, are described by Equations 9:

$$M_1 = \frac{\lambda_2\sqrt{\alpha_1}}{\lambda_1\sqrt{\alpha_2}+\lambda_2\sqrt{\alpha_1}} \tag{9'}$$

$$M_2 = \frac{\lambda_1\sqrt{\alpha_2}}{\lambda_1\sqrt{\alpha_2}+\lambda_2\sqrt{\alpha_1}} \tag{9''}$$

The integral can be solved as below:

$$\int_0^t \frac{1}{\sqrt{t}\sqrt{t-\tau}}\,d\tau = \left| \begin{array}{l} \tau = t\sin^2 s \\ d\tau = 2t\sin s \cdot \cos s\, ds \end{array} \right| = \int_0^{\pi/2} 2\,ds = \pi$$

---

and Equations 8 and 9 now yield:

$$T_c = T_1(0,t) = T_2(0,t) = T_1' - (T_1' - T_2')\cdot M_1 = T_2' + (T_1' - T_2')\cdot M_2$$
$$= \frac{\lambda_1\sqrt{\alpha_2}T_1' + \lambda_2\sqrt{\alpha_1}T_2'}{\lambda_1\sqrt{\alpha_2}+\lambda_2\sqrt{\alpha_1}} = \frac{T_1'\sqrt{\lambda_1 c_{p1} g_1} + T_2'\sqrt{\lambda_2 c_{p2} g_2}}{\sqrt{\lambda_1 c_{p1} g_1} + \sqrt{\lambda_2 c_{p2} g_2}} \tag{10}$$

where: $y_1 = y_2 = 0$ and $t > 0$

It also follows from Equations 8 and 9 that the thermal gradients as a function of time and distance from the contacted surfaces are:

$$\frac{\partial T_1}{\partial y_1}(y_1,t) = \frac{M_1 y_1}{2\pi\alpha_1}(T_1' - T_2')\int_0^t \frac{1}{\sqrt{\tau}\sqrt{(t-\tau)^3}} \exp\left[-\frac{y_1^2}{4\alpha_1(t-\tau)}\right] d\tau \tag{11'}$$

$$\frac{\partial T_2}{\partial y_2}(y_2,t) = -\frac{M_2 y_2}{2\pi\alpha_2}(T_1' - T_2')\int_0^t \frac{1}{\sqrt{\tau}\sqrt{(t-\tau)^3}} \exp\left[-\frac{y_2^2}{4\alpha_2(t-\tau)}\right] d\tau \tag{11''}$$

Equations 11 can readily be solved, yielding:

$$\frac{\partial T_1}{\partial y_1}(y_1,t) = -\frac{M_1}{\sqrt{t\alpha_1\pi}}(T_1' - T_2')\exp\left[-\frac{y_1^2}{4\alpha_1 t}\right] \tag{12'}$$

$$\frac{\partial T_2}{\partial y_2}(y_2,t) = -\frac{M_2}{\sqrt{t\alpha_2\pi}}(T_1' - T_2')\exp\left[-\frac{y_2^2}{4\alpha_2 t}\right] \tag{12''}$$

where: $y_1 < 0$, $y_2 > 0$, $t > 0$

The thermal gradient's uniformity (Equation 12) was derived for four reasons:

1. While the y_1, y_2 are variable in the spatial interval $(-\infty, 0^-)$, $(0^+, \infty)$ and $t > 0$ is stationary, the limits of the functions are, respectively:

$$\lim_{y_1 \to -\infty} \frac{\partial T_1}{\partial y_1}(y_1,t) = 0 \qquad \lim_{y_1 \to 0^-} \frac{\partial T_1}{\partial y_1}(y_1,t) = -M_1 \frac{(T_1' - T_2')}{\sqrt{t\alpha_1 \pi}}$$

$$\lim_{y_2 \to +\infty} \frac{\partial T_2}{\partial y_2}(y_2,t) = 0 \qquad \lim_{y_2 \to 0^+} \frac{\partial T_2}{\partial y_2}(y_2,t) = -M_2 \frac{(T_1' - T_2')}{\sqrt{t\alpha_2 \pi}}$$

The thermal gradients (Equations 12) reach extreme values:

$$\frac{\partial T_{ex1}}{\partial y_1}(0^-,t) = -M_1 \frac{T_1' - T_2'}{\sqrt{t\alpha_1 \pi}} \tag{13'}$$

$$\frac{\partial T_{ex2}}{\partial y_2}(0^+,t) = -M_2 \frac{T_1' - T_2'}{\sqrt{t\alpha_2 \pi}} \tag{13''}$$

where: $y_1 = 0^-, y_2 = 0^+$

The function of Equations 12 have the inflection points and reach values:

$$\frac{\partial T_1}{\partial y_2}(y_{1p},t) = -M_1 \frac{T_1' - T_2'}{\sqrt{t\alpha_1 e\pi}} \tag{14'}$$

$$\frac{\partial T_2}{\partial y_2}(y_{2p},t) = -M_2 \frac{T_1' - T_2'}{\sqrt{t\alpha_2 e\pi}} \tag{14''}$$

where:

$$y_{1p} = -\sqrt{2t\alpha_1} \tag{15'}$$

$$y_{2p} = \sqrt{2t\alpha_2} \tag{15''}$$

---

2. While y_1, y_2 are variable in the spatial interval $(-\infty, 0^-)$, $(0^+, \infty)$ and $t = 0^+$ is stationary, the maximum (in absolute values) thermal gradients (Equations 12) at search distances y_1 or y_2 from the contact surface are determined by equations:

$$\frac{\partial T_1}{\partial y_1}(y_1,0^+) = M_1 \frac{\sqrt{2}}{y_1\sqrt{e\pi}}(T_1' - T_2') = 0.4839414 \frac{M_1}{y_1}(T_1' - T_2') \tag{16'}$$

$$\frac{\partial T_2}{\partial y_2}(y_2,0^+) = -M_2 \frac{\sqrt{2}}{y_2\sqrt{e\pi}}(T_1' - T_2') = -0.4839414 \frac{M_2}{y_2}(T_1' - T_2') \tag{16''}$$

where: $y_1 \to 0^-$, $y_2 \to 0^+$

The limits of functions (Equations 16) in the extreme distances interval are, respectively:

$$\lim_{y_1 \to -\infty} \frac{\partial T_1}{\partial y_1}(y_1,0^+) = 0 \qquad \lim_{y_1 \to 0^-} \frac{\partial T_1}{\partial y_1}(y_1,0^+) = -\infty$$

$$\lim_{y_2 \to +\infty} \frac{\partial T_2}{\partial y_2}(y_2,0^+) = 0 \qquad \lim_{y_2 \to 0^+} \frac{\partial T_2}{\partial y_2}(y_2,0^+) = \infty$$

The functions have any inflection points and extreme values.

3. While t is variable in the time interval $(0, \infty)$ and $y_1 < 0$, $y_2 > 0$ are stationary, the limits of functions in the extreme time interval are:

$$\lim_{t \to 0^+} \frac{\partial T_1}{\partial y_1}(y_1,t) = 0 \qquad \lim_{t \to \infty} \frac{\partial T_1}{\partial y_1}(y_1,t) = 0$$

$$\lim_{t \to 0^+} \frac{\partial T_2}{\partial y_2}(y_2,t) = 0 \qquad \lim_{t \to \infty} \frac{\partial T_2}{\partial y_2}(y_2,t) = 0$$

The thermal gradients (Equations 12) reach extreme values:

$$\frac{\partial T_{ex1}}{\partial y_1}\left(y_1, \frac{y_1^2}{2\alpha_1}\right) = M_1 \frac{\sqrt{2}}{y_1\sqrt{e\pi}}(T_1' - T_2') \tag{17'}$$

$$\frac{\partial T_{ex2}}{\partial y_2}\left(y_2, \frac{y_2^2}{2\alpha_2}\right) = -M_2 \frac{\sqrt{2}}{y_2\sqrt{e\pi}}(T_1' - T_2') \tag{17''}$$

at the moment:

$$t_{ex1} = \frac{y_1^2}{2\alpha_1} \tag{18'}$$

$$t_{ex2} = \frac{y_2^2}{2\alpha_2} \tag{18''}$$

The inflection points reach values:

$$\frac{\partial T_{1(1p)}}{\partial y_1}(y_1, t_{1(1p)}) = M_1 \frac{T_1' - T_2'}{y_1\sqrt{\pi}\sqrt{\frac{1}{2} - \frac{\sqrt{6}}{6}}} \exp\left[-\frac{3+\sqrt{6}}{2}\right] \tag{19'_{1p}}$$

$$\frac{\partial T_{1(2p)}}{\partial y_1}(y_1, t_{1(2p)}) = M_1 \frac{T_1' - T_2'}{y_1\sqrt{\pi}\sqrt{\frac{1}{2} + \frac{\sqrt{6}}{6}}} \exp\left[-\frac{3-\sqrt{6}}{2}\right] \tag{19'_{2p}}$$

$$\frac{\partial T_{2(1p)}}{\partial y_2}(y_2, t_{2(1p)}) = -M_2 \frac{T_1' - T_2'}{y_2\sqrt{\pi}\sqrt{\frac{1}{2} - \frac{\sqrt{6}}{6}}} \exp\left[-\frac{3+\sqrt{6}}{2}\right] \tag{19''_{1p}}$$

$$\frac{\partial T_{2(2p)}}{\partial y_2}(y_2, t_{2(2p)}) = -M_2 \frac{T_1' - T_2'}{y_2\sqrt{\pi}\sqrt{\frac{1}{2} + \frac{\sqrt{6}}{6}}} \exp\left[-\frac{3-\sqrt{6}}{2}\right] \tag{19''_{2p}}$$

---

at the moment:

$$t_{1(1p)} = \left[\frac{1}{2} - \frac{\sqrt{6}}{6}\right] \cdot \frac{y_1^2}{\alpha_1} \qquad t_{1(2p)} = \left[\frac{1}{2} + \frac{\sqrt{6}}{6}\right] \cdot \frac{y_1^2}{\alpha_1} \tag{20'_{1p}, 20'_{2p}}$$

$$t_{2(1p)} = \left[\frac{1}{2} - \frac{\sqrt{6}}{6}\right] \cdot \frac{y_2^2}{\alpha_2} \qquad t_{2(1p)} = \left[\frac{1}{2} + \frac{\sqrt{6}}{6}\right] \cdot \frac{y_2^2}{\alpha_2} \tag{20''_{1p}, 20''_{2p}}$$

---

4. While t is variable in the time interval (0, ∞) and y_1, y_2 are stationary, the maximum (in absolute values) thermal gradients (Equations 12) at the search moment and the optional point of planes, which are parallel to the contact surface and are at a distance $y_1 = 0^-$ or $y_2 = 0^+$, are determined by equations:

$$\frac{\partial T_1}{\partial y_1}(0^-, t) = -M_1 \frac{T_1' - T_2'}{\sqrt{\alpha_1 t \pi}} \tag{21'}$$

$$\frac{\partial T_2}{\partial y_2}(0^+, t) = -M_2 \frac{T_1' - T_2'}{\sqrt{\alpha_2 t \pi}} \tag{21''}$$

where $t \to 0$

The limits of functions (Equations 21) in the extreme time interval are, respectively:

$$\lim_{t \to 0^+} \frac{\partial T_1}{\partial y_1}(0^-, t) = -\infty \qquad \lim_{t \to \infty} \frac{\partial T_1}{\partial y_1}(0^-, t) = 0$$

$$\lim_{t \to 0^+} \frac{\partial T_2}{\partial y_2}(0^+, t) = -\infty \qquad \lim_{t \to \infty} \frac{\partial T_2}{\partial y_2}(0^+, t) = 0$$

The functions (Equations 21) have any inflection points and extreme values.

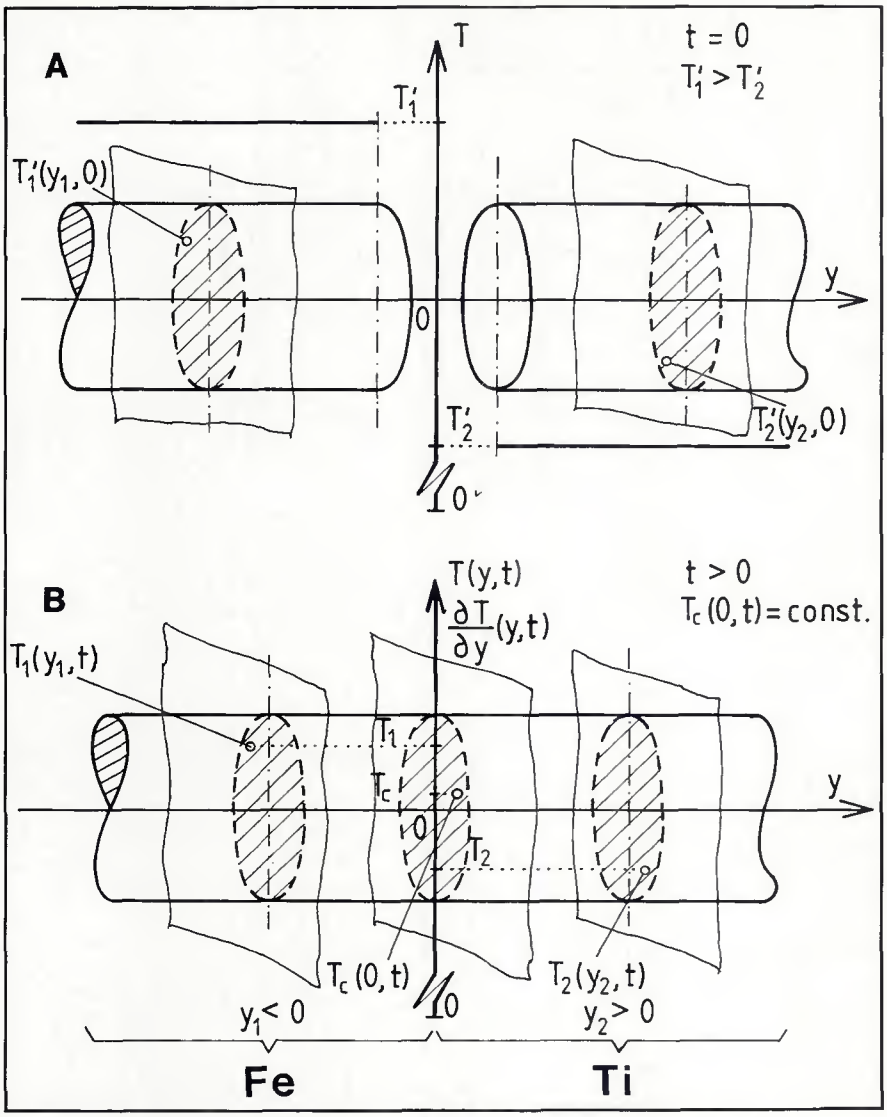

Fig. 4 — Illustrations of the model to calculate the temperatures T_1 and T_2 and the gradient distribution in the boundary layers of two semi-infinite bars. Symbols used in the calculations: A — Both parts are separately heated to different temperatures T_1' and T_2', viz., $t = 0$; B — They are brought into contact forming the surface of contact S_c, viz., $t > 0$

Evaluation of the Temperature, Thermal Gradient and Heat Flux Density Variation for the Unlimited Fe-Ti Binary Bar

In the present investigation, the DFW/TS of technically pure iron to titanium was performed as an example of joining dissimilar metal combinations which form intermetallic compounds. Both metals have allotropic variations at high temperature — Fig. 5. Iron and titanium form a binary system characterized by unlimited solubility of components in a liquid state, by a limited solubility in the solid state and by two intermetallic phases, and they are also stable at low temperature, *viz.*, FeTi and Fe_2Ti (Ref. 14). Based on the analysis of the structures of both metals at high temperature and of the diffusion coefficients (Ref. 15), in the present calculation it was accepted that the iron part is heated to a higher temperature. The temperatures of both parts were selected so that the contact temperature T_c was always higher than the transformation point $Ti_\alpha \rightleftharpoons Ti_\beta$, *viz.*, 1166 K — Fig. 5.

The characteristic of the thermal effects during DFW/TS was made in this case when the unlimited binary bar is composed of iron and titanium parts, the difference in temperature of the parts was 300°, and the iron and titanium were heated separately, but at the same time, to 1423 K and 1123 K, respectively, before joining. The calculations take into account the variations of λ, c_p and g of both metals with respect to temperature (Ref. 16). Simultaneously, because at high temperature the variations are not great, the approximation was made and the average values from the temperature ranges were used — Table 1. The contact temperature T_c was calculated on the basis of Equations 10. The temperature quantities were treated numerically on the basis of Equations 8 and 9, which gave the reason for the drawing of temperature variations in the stationary time — Fig. 6. The curves afford possibilities for finding the quantity of the temperature of an arbitrary point in the specified time, measured from the moment of contact of the surfaces. For example, the point y_2, which is $1 \cdot 10^{-5}$ m distant from the place of connected surfaces 0, after time $t = 1 \cdot 10^{-4}$ s, has increased the temperature from 1123 to 1268 K — Fig. 6, Curve 5″. At this time, at the distance $y_2 = 1 \cdot 10^{-6}$ m, the point temperatures have risen to 1303 and 1310 K. At the other points, the temperatures changed in the same manner. (Because the distances y_1 and y_2 on Figs. 6, 7 and 10 are appointed in logarithmic scale, *viz.*, without zero, the iron and titanium diagrams have been removed.)

Figure 7 illustrates the thermal gradient distribution in the same conditions as for temperature variation, *viz.*, in the specified time and at a variable distance from 0. Curves 2, 3 and 4 (Equations 12) are attributed to the definite time $t = 2 \cdot 10^{-5}$, $t = 1 \cdot 10^{-4}$, $t = 1 \cdot 10^{-3}$ s, respectively. The characteristic of the variation of one of them can estimate the depth of layers and intensity of thermal effects which have proceeded in it. For example, at the moment $t = 1 \cdot 10^{-4}$ s (Curve 3″), the extreme value of the thermal gradient when $y_2 = 0^+$ is equal to −4 232 242°/m (Equation 13″); at the distance $y_{2p} = 3.52 \cdot 10^{-5}$ m (Equation 15″) it is equal to −2 566 985°/m (Equation 14″); and next, in absolute values, it quickly diminishes and reaches values of −75 339°/m at the distance $y_2 = 1 \cdot 10^{-4}$ m (Equation 12″). At this time, the point temperature $y_{2p} = 3.52 \cdot 10^{-5}$ m amounts to 1179 K (Fig. 6, Curve 5″) and simultaneously rises. At the times $t = 1 \cdot 10^{-3}$ s and $t = 1 \cdot 10^{-2}$ s, it reaches 1264 and 1303 K, respectively (Fig. 6, Curves 6″, 7″). Curves 2″ and 4″ (Fig. 7) show the thermal gradient variations which have different values at the other moments in time. Curve 1″ (Fig. 7) illustrates the extreme values of the thermal gradients attained at different points when $y_2 \rightarrow 0$ and $t = 0^+$. The values were calculated on the basis of Equation 16″. One ought to emphasize that the inflection points l_p (Equations 14, 15) of Curves 2, 3 and 4 are on Curve 1, which has been drawn on the basis of Equation 16. That is why Equation 16 will be used to calculate the variables of the joining process with DFW/TS.

Figures 8 and 9 illustrate the thermal gradient distribution as a time function at definite points on the iron and titanium parts, respectively. For example, at the point $y_2 = 1 \cdot 10^{-5}$ m and at the time $t = 1 \cdot 10^{-6}$ s, the thermal gradient in the colder, titanium part amounts to −753

390°/m and, in absolute values, it increases (Equation 12″) (Fig. 9, Curve 2″). In the time $t_{ex} = 8.06 \cdot 10^{-6}$ s (Equation 18″), it attains the extreme value equal to −9 043 514°/m (Equation 17″). Next, the thermal gradient in absolute values is quickly diminished. After $t = 1 \cdot 10^{-4}$ and $t = 1 \cdot 10^{-3}$ s, the thermal gradients attain the values equal to −4 065 136° and −1 332 972°/m, respectively. This variation of the thermal gradient in time corresponds with the point temperature $y_2 = 1 \cdot 10^{-5}$ m, which increases at the time $t = 1 \cdot 10^{-6}$ s, and after the times $t = 2 \cdot 10^{-5}$, $t = 1 \cdot 10^{-4}$ and $t = 1 \cdot 10^{-3}$ s, it attains 1192, 1268 and 1294 K, respectively (Fig. 6, Curves 4″, 5″ and 6″). Later, at the time $t = 1 \cdot 10^{-2}$, the thermal gradient is equal to −423 054°/m, and the temperature is 1303 K. At the points $y_2 = 5 \cdot 10^{-5}$ and $y_2 = 1 \cdot 10^{-4}$ m (Fig. 9, Curves 3″, 4″), the thermal gradient changes in the same manner, but the corresponding, absolute values are lower. Curve 1″ (Fig. 9) illustrates the maximum values of the thermal gradient attained at the definite points $y_2 = 0^+$ when $t \to 0$. The shape of this curve is similar to Curve 1″ (Fig. 7), but this diagram has the time axis. The character and evaluation of the thermal gradient are similar, and the maximum intensity of the thermal effect is characterized in the thermal boundary layer of both metals. The values were calculated on the basis of Equation 21″. Equation 21 will be used to calculate the variables of the joining process with DFW/TS.

Similarly, in the hotter iron part, at the point $y_1 = 1 \cdot 10^{-5}$ m (Fig. 8), the thermal gradient increases in absolute values, and at the times $t = 1 \cdot 10^{-6}$ s (Equation 12′) and $t_{ex} = 7.55 \cdot 10^{-6}$ s (Equation 18′), it attains −567 652° and −5 474 578° /m, respectively. Next, the thermal gradient diminishes in absolute values, and at the times $t = 2 \cdot 10^{-5}$, $t = 1 \cdot 10^{-4}$ and $t = 1 \cdot 10^{-3}$ s, it attains the values equal to −4 592 736°; −2 388 953° and −781 578°/m, respectively (Equation 12′). The temperature of this point diminishes in time function and attains 1422, 1369, 1352, 1327 and 1313 K, respectively (Fig. 6, Curves 3′, 4′, 5′ and 6′). In the iron

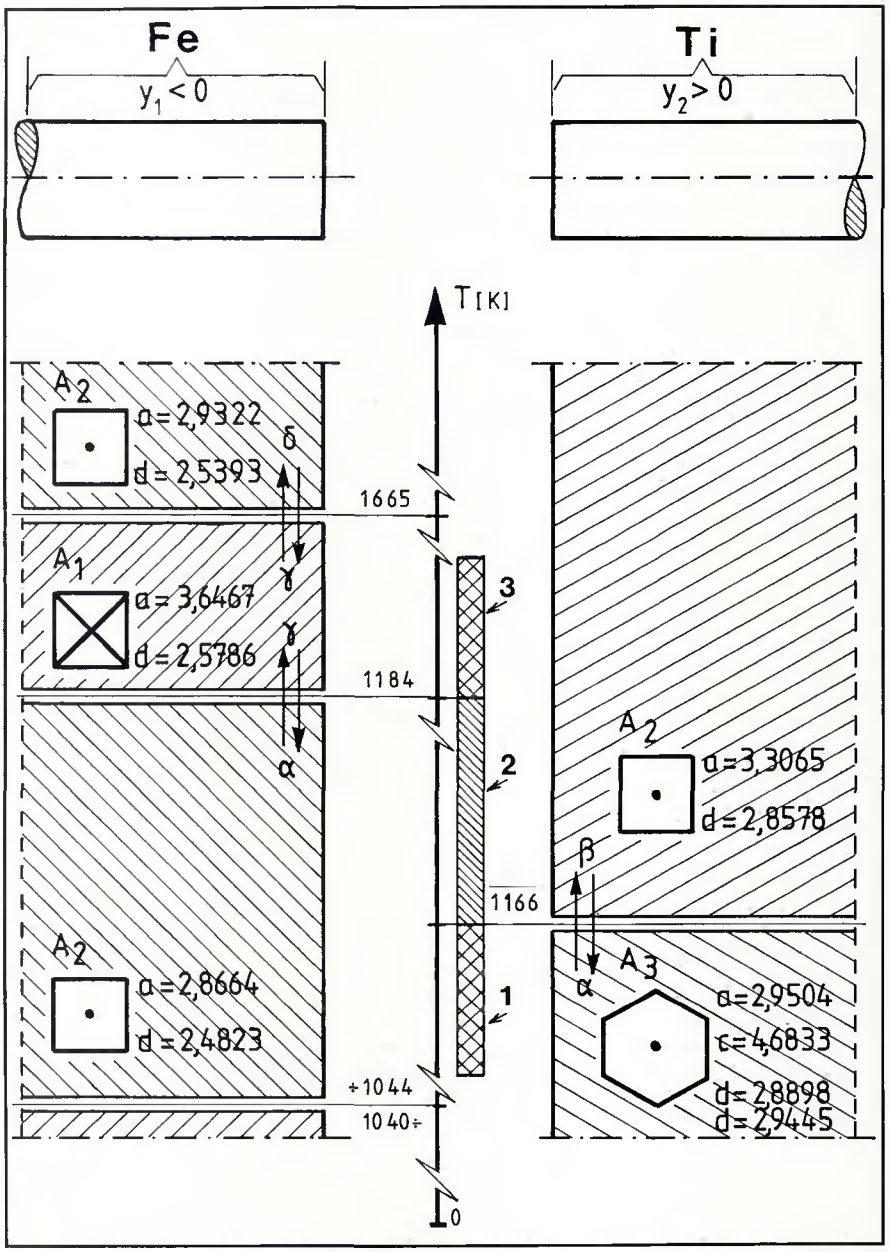

Fig. 5—Illustration of criteria for selecting the contact temperature for the DFW/TS process joining iron and titanium as determined by the crystalline formation. The temperature ranges 1, 2 and 3 have been separated for investigation. Under the symbol for the types of unit cells of crystal lattices, the parameters a and c of the lattice and the interatomic distances d are quoted in angstroms (Å) (Refs. 15, 20)

Table 1—The Values of Thermal Conductivities (λ), Specific Heats (c_p), Specific Gravities (g), and Thermal Conductances (α) of Iron and Titanium Heated to Different Temperatures. (The values for transfer coefficients M_1 and M_2 are also given)

	Fe				M_1	M_2	Ti			
Temperature [K]	λ_1 [W/m·K]	c_{p1} [J/kg·K]	g_1 [kg/m³]	α_1 Equation 4′ [m²/s]	Equation 9′	Equation 9″	λ_2 [W/m·K]	c_{p2} [J/kg·K]	g_2 [kg/m³]	α_2 Equation 4″ [m²/s]
298	73	439	7870	$2.1129 \cdot 10^{-5}$	0.3213467	0.6786533	24	523	4505	$1.0186 \cdot 10^{-5}$
1200	29	585	7668	$6.4648 \cdot 10^{-6}$	0.3747669	0.6252271	17	628	4378	$6.1832 \cdot 10^{-6}$
1300[a]	29	578	7581	$6.6182 \cdot 10^{-6}$	0.3770827	0.6229069	17	628	4362	$6.2058 \cdot 10^{-6}$
1400	30	615	7531	$6.4772 \cdot 10^{-6}$	—	—	—	—	—	—

[a]The values used in the present calculations.

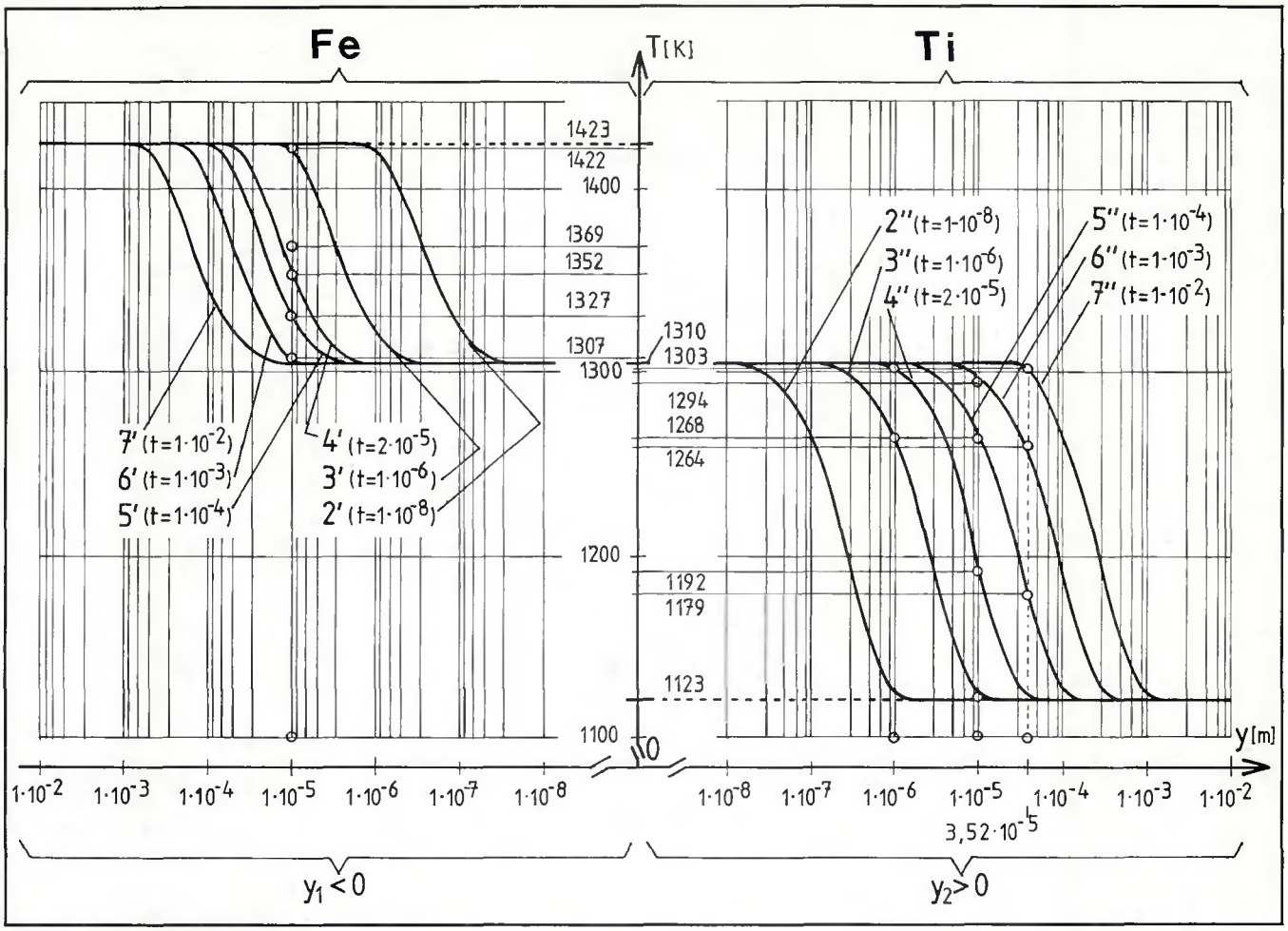

Fig. 6 – Temperature distribution in the boundary layer of iron and titanium parts which have been brought into contact after heating to different temperatures $T_1' = 1423$ K and $T_2' = 1123$ K, respectively. The curves illustrate the temperature changes at the distances y_1 and y_2 from contact surface for different values of time after contact, viz., $t > 0$ (Fig. 4B)

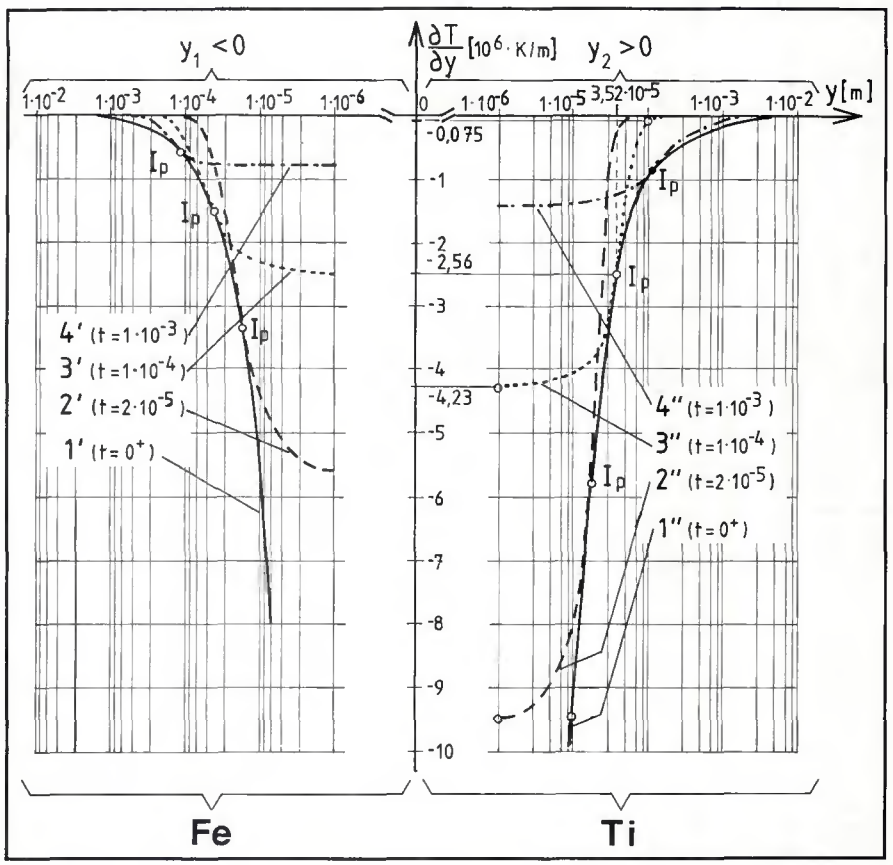

Fig. 7 – Thermal gradient distribution in the boundary layer of iron and titanium parts which have been brought into contact after heating to temperatures $T_1' = 1423$ K and $T_2' = 1123$ K, respectively. The curves illustrate the thermal gradient changes at the distances y_1 and y_2 from the contact surface for different values of time after contact, viz., $t > 0$. I_p – the inflection points of Curves 2, 3 and 4

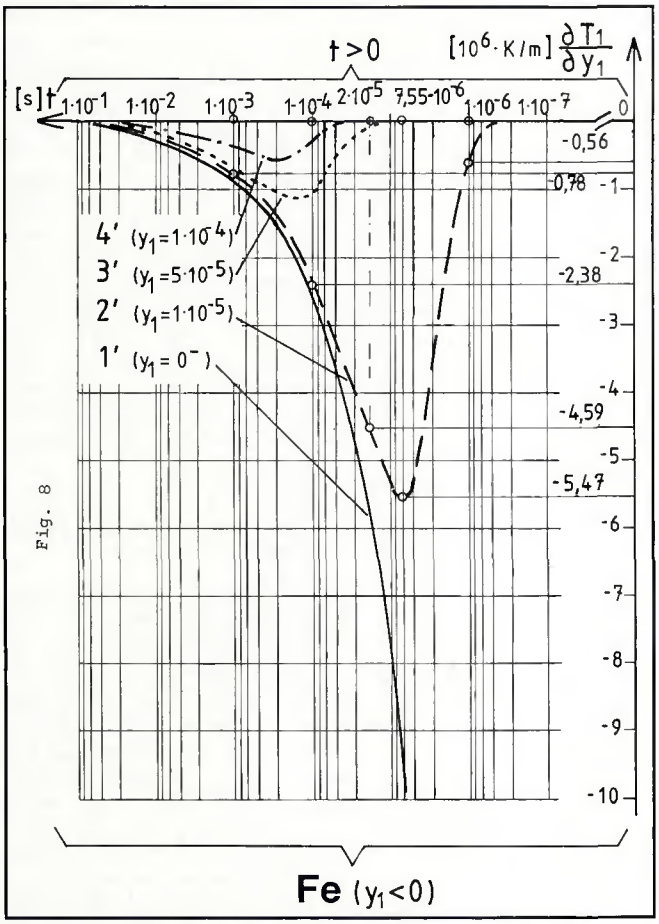

Fig. 8 — Character of thermal gradient variation in the boundary layer of the iron part as a function of time for different values of distance y_1. Thermal gradient values in the iron part were calculated when the iron and titanium parts have been brought into contact after heating to temperatures $T_1' = 1423$ K and $T_2' = 1123$ K, respectively

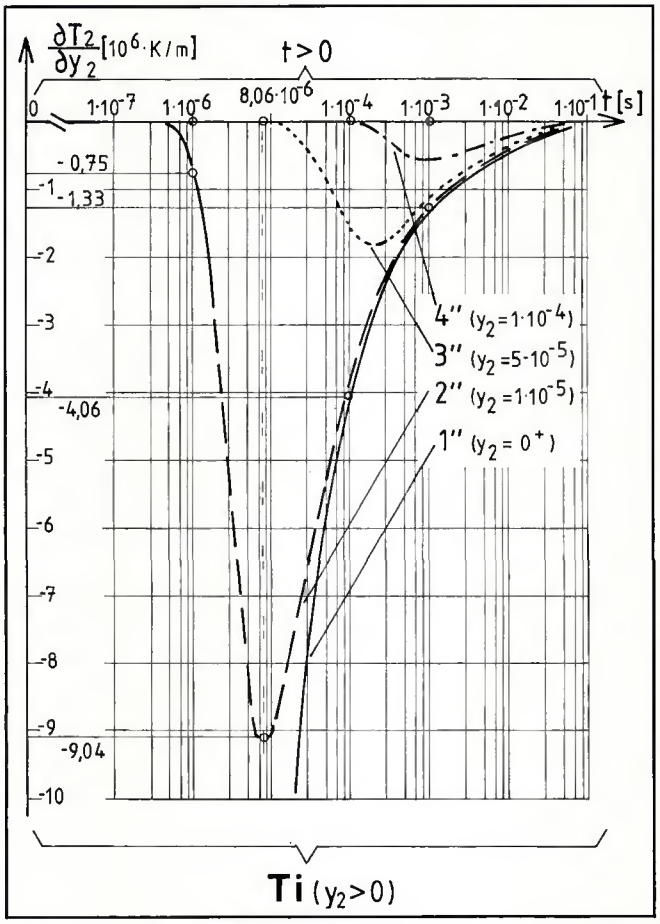

Fig. 9 — Character of thermal gradient variation in the boundary layer of the titanium part as a function of time for different values of distance y_2. Thermal gradient values in the titanium part were calculated when iron and titanium parts have been brought into contact after heating to temperatures $T_1' = 1423$ K and $T_2' = 1123$ K, respectively

part (Fig. 8), the thermal gradient variation was described by the additional time axis, which is in direct contrast to the analogical time axis for the thermal gradient variation of the titanium part in Fig. 9. This was done in graphic reference to Figs. 6, 7 and 10. The equations which were used for the above calculations were also employed for the data calculations of DFW/TS.

The values of the thermal gradient in the boundary layer are dependent on the levels and temperature difference of the parts. Figure 10 illustrates these variations. For instance, when iron is heated higher than titanium by 100°, 200° and 300°, the temperature of titanium remains at 1123 K. The values were calculated on the basis of Equations 9 and 16. The calculations for the iron part of an unlimited bar were made in a similar manner. The evaluations are presented in Figs. 6, 7, 8 and 10.

The instantaneous, maximum values of heat flux density in the surface layer of two parts which have been heated to different temperatures before contact can be evaluated on the grounds of the Fourier law (Formula 22, Ref. 17):

$$q_{max} = -\lambda \frac{\partial T}{\partial y} \qquad (22)$$

The heat flux density was derived for two reasons:

1. While the distance y_1 and y_2 are variable, Formula 22 with Equations 16 yields:

$$q_{y_1 max} = -\sqrt{\frac{2}{\pi e}} \cdot \frac{\lambda_1 M_1}{y_1}(T_1' - T_2') =$$

$$-0.4839414 \frac{\lambda_1 M_1}{y_1}(T_1' - T_2') \qquad (23')$$

$$q_{y_2 max} = \sqrt{\frac{2}{\pi e}} \cdot \frac{\lambda_2 M_2}{y_2}(T_1' - T_2') =$$

$$0.4839414 \frac{\lambda_2 M_2}{y_2}(T_1' - T_2') \qquad (23'')$$

where: λ (thermal conductivity) and M (transfer coefficient described in Equation 9) are variable in the temperature.

Equation 23″ defines the momentary, maximum value of the heat flux density in the surface layer of the colder part as the distance function y_2 from the connected surfaces. For example, when the iron and titanium parts were heated to 1423 and 1123 K, respectively, the difference in temperature before joining was 300°. After pressing both parts to each other, the maximum heat flux density obtained in the titanium colder part at the distance $y_2 = 1 \cdot 10^{-6}$ m from connected surfaces is $q_{y_2 max} = 1.537 \cdot 10^9$ kW/m² (Fig. 11, Line 3″).

Apart from this, it is possible to select the difference $T_1' - T_2'$ and the level of the temperature heating for both parts. It creates the possibility for fine control of the heat energy quantity essential to joining, *viz.*, the thermal spike. For example, at the distance $y_2 = 1 \cdot 10^{-6}$ m from the contact, when $T_1' - T_2' = 300°$, 200° or 100°, the heat flux density amounts to $1.537 \cdot 10^9$, $1.02 \cdot 10^9$ or $5.12 \cdot 10^8$ kW/m², respectively, for the elementary surface of the colder part. Temperature of the titanium part T_2' is a constant 1123 K — Table 2 and Fig. 11, Lines 1″, 2″, 3″.

2. While the time is variable, Formula 22 with Equations 21 yields:

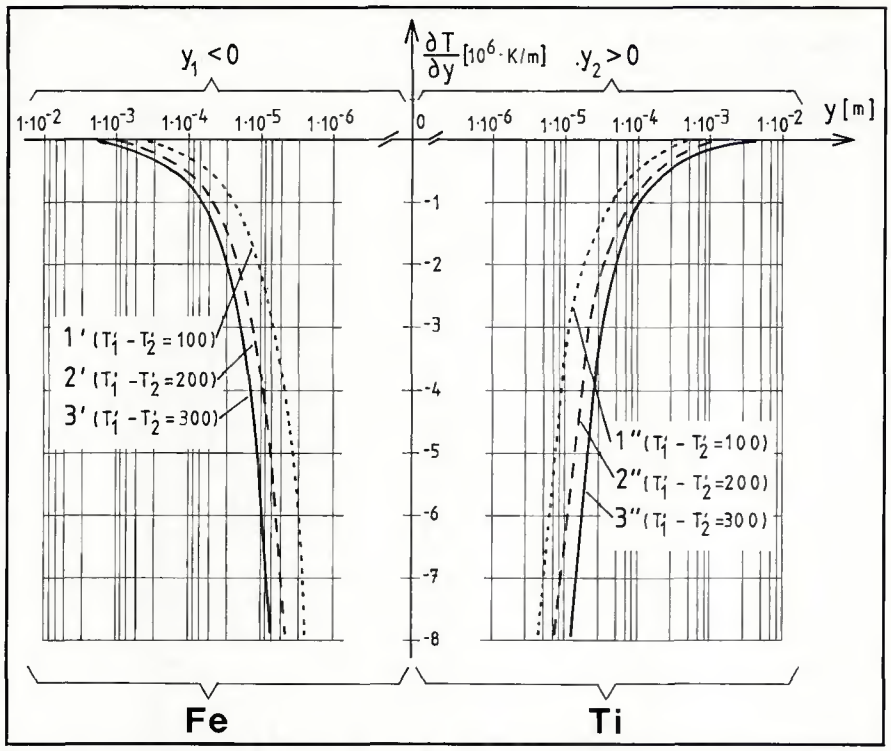

Fig. 10—Comparison of the maximum values of the thermal gradient at the distances y_1 and y_2 from the contact surface as a function of the difference in heating temperature for both parts before pressure is applied. Curves 1, 2 and 3 were calculated for the cases when the differences are 100°, 200° and 300°, respectively. Temperature of the titanium part was constant: $T_2' = 1123$ K

$$q_{1t\,max} = \frac{\lambda_1 M_1}{\sqrt{\alpha_1 t \pi}}(T_1' - T_2') \qquad (24')$$

$$q_{2t\,max} = \frac{\lambda_2 M_2}{\sqrt{\alpha_2 t \pi}}(T_1' - T_2') \qquad (24'')$$

where: α, λ and M are variable in the temperature.

Equation 24" defines the momentary, maximum value of the heat flux density in the surface layer of the colder part in the time function. The values depend on the heating temperatures T_1' and T_2' of both parts, lapse of the time after contact and on α_2, λ_2, M_2—Fig. 12 and Table 3.

Comparison of values has been given by Equations 23" and 24", enabling the values of the thermal effects in the surface layer of the connection and the variability as a time function to be calculated. For example, when the iron and titanium parts have been heated to 1423 and 1123 K, respectively, and have been pressed to each other, for the colder part at the distances of $y_2 = 1 \cdot 10^{-6}$ and $y_2 = 1 \cdot 10^{-4}$ m, the momentary, maximum values of the thermal gradient are $-9.0435 \cdot 10^7$ and $-9.0435 \cdot 10^5$ °/m (Equation 21"), and the heat flux densities are $1.5373 \cdot 10^9$ and $1.5373 \cdot 10^7$ kW/m², respectively (Equation 24")—Tables 2, 3 and Figs. 11, 12. These values for the thermal gradient (also the heat flux density) were reached in the times of $t = 2.1901 \cdot 10^{-7}$ and $t = 2.1901 \cdot 10^{-3}$ s, respectively—Table 3. The time was calculated on the basis of Equations 24" or 25.

Thus, in DFW/TS, it is possible to generate the instantaneous, very large values of heat flux density flow by contacting the surfaces of members to be joined. The momentary heat flux density can be controlled by changing the levels, and especially the temperature difference, of the parts. With the aim of demonstrating a comparison of the instantaneous heat flux density generated in DFW/TS, the values are presented against the other fusion welding processes—Figs. 11 and 12.

Evaluation of the DFW/TS Process Variables for the Unlimited Fe-Ti Binary Bar

Similar to the conventional DFW, the basic variables in the procedure for DFW/TS are: temperature, the time of welding, and pressure. The selection of heating temperatures for both parts was made based on the analysis of the properties of the metal parts joined at high temperatures. The following factors were taken into consideration: temperatures of transformation points, crystalline structure, diffusion coefficients, heat compressive strength, and physical properties λ, c_p and g at high temperatures. As a rule, it can be said that: 1) the part made from the metal which has the higher transformation temperature, larger diffusion coefficient and heat compressive strength ought to be heated to the higher temperature; 2) the level and difference of heating temperatures are dependent on the transformation temperature points, crystalline structures, and values of λ, c_p and g at high temperatures.

The second variable, the welding time, depends on the properties of the joined metals. Variation of the temperature in the boundary layer as a time function needs a detailed discussion on the separate periods of the heating procedure in DFW/TS. Control of these periods raises

Table 2—Instantaneous Maximum Value of the Thermal Gradient and Heat Flux Density in the Surface Layer of the Titanium Part as a Function of the Distance y_2 and the Difference in Temperatures $T_1' - T_2'$

λ_2 (in 1300 K) [W/m · K]	y_2 [m]	G_{2t} [degrees/m] (Equation 16") $T_1' - T_2'$ 300°	200°	100°	$q_{y_2\,max}$ [kW/m²] (Equation 23) $T_1' - T_2'$ 300°	200°	100°
17	$1 \cdot 10^{-7}$	$-9.0435 \cdot 10^8$	$-6.029 \cdot 10^8$	$-3.0145 \cdot 10^8$	$1.5373 \cdot 10^{10}$	$1.0249 \cdot 10^{10}$	$5.1246 \cdot 10^9$
	$1 \cdot 10^{-6}$	$-9.0435 \cdot 10^7$	$-6.029 \cdot 10^7$	$-3.0145 \cdot 10^7$	$1.5373 \cdot 10^9$	$1.0249 \cdot 10^9$	$5.1246 \cdot 10^8$
	$1 \cdot 10^{-5}$	$-9.0435 \cdot 10^6$	$-6.029 \cdot 10^6$	$-3.0145 \cdot 10^6$	$1.5373 \cdot 10^8$	$1.0249 \cdot 10^8$	$5.1246 \cdot 10^7$
	$4.2 \cdot 10^{-5}$	$-2.1532 \cdot 10^6$	$-1.435 \cdot 10^6$	$-7.1774 \cdot 10^5$	$3.6604 \cdot 10^7$	$2.4403 \cdot 10^7$	$1.2201 \cdot 10^7$
	$1 \cdot 10^{-4}$	$-9.0435 \cdot 10^5$	$-6.029 \cdot 10^5$	$-3.0145 \cdot 10^5$	$1.5373 \cdot 10^7$	$1.0249 \cdot 10^7$	$5.1246 \cdot 10^6$
	$1 \cdot 10^{-3}$	$-9.0435 \cdot 10^4$	$-6.029 \cdot 10^4$	$-3.0145 \cdot 10^4$	$1.5373 \cdot 10^6$	$1.0249 \cdot 10^6$	$5.1246 \cdot 10^5$

the possibility of influencing the joint microstructure and the plastic deformation range. Depending on the heating procedure of both parts, two cases are distinguishable. The first is applied when the heating of separate members makes the diffusion reaction, *viz.*, formation of intermetallic compounds, impossible in the preweld interval before the welding temperature is reached. The heating of separate members profits by the introduction of the large thermal gradient in the boundary layer, *viz.*, the intensification of thermal diffusion mass transfer. The continuation of the heating process at a definite, constant temperature T_c after pressure brings the joint to perfection.

In this case, the time of DFW/TS includes three periods—Fig. 13A. The first, t_i interval of the thermal surge time is measured from the moment of pressure to the moment at which the contact temperature T_c at the definite distance y_i from the surface contact is obtained. The interval of time t_i is defined as the time of thermal surge heating up for the specified thickness y_i of the boundary layer of the colder part to the contact temperature T_c. The second period, t_γ, is an interval of time measured from the moment at which the boundary layer had been up to the contact temperature T_c to the moment that the temperature of the parts begins to drop after switching off the heating. The t_γ period is defined as the time of diffusion welding at the constant temperature T_c. The third period, t_μ, of cooling down is measured at the moment when the temperature drop of the parts begins. The t_μ period defines the cooling time from one temperature to the other. In this example, it is the time from the contact temperature T_c to the assumed temperature T_μ. The periods t_i, t_γ and t_μ define the dwell time of diffusion welding $t_{DFW/TS}$ at the temperatures higher than T_μ.

The second case is applied when the heating of separate members, similar to the situation in the first case, makes the diffusion reaction impossible. The maxi-

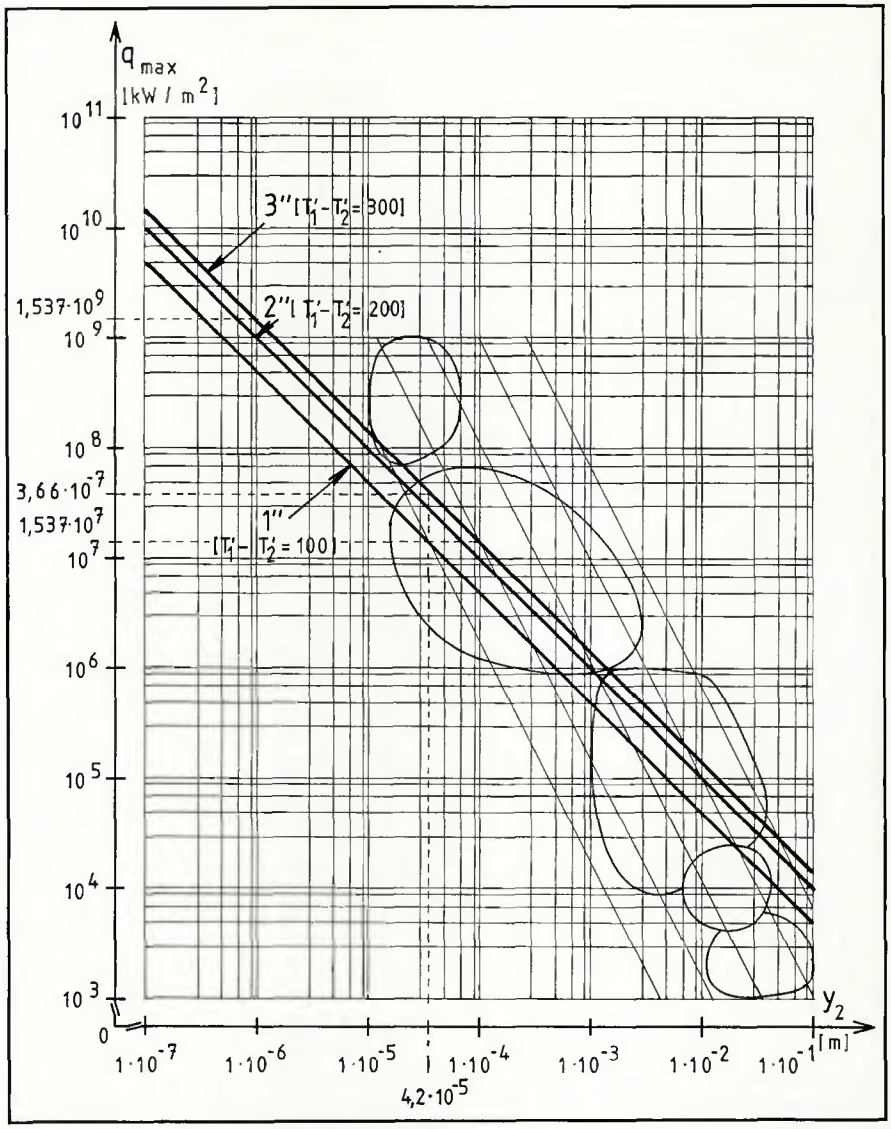

Fig. 11—Instantaneous maximum value of the heat flux density in the surface layer of the titanium part as a function of distance y_2 and the temperature difference $T_1' - T_2'$, to which the parts have been heated before pressing. Temperature of the titanium part was constant: $T_2' = 1123$ K. The values shown are presented against a background of constant time, $t = 0^+$, and maximum heat flux densities obtained with other fusion welding processes (see Fig. 1)

Table 3—Instantaneous Maximum Value of the Thermal Gradient and Heat Flux Density in the Surface Layer of the Titanium Part as a Function of Time and Difference in Temperatures $T_1' - T_2'$

λ_2 (in 1310 K) $\left[\frac{W}{m \cdot K}\right]$	t [s]	G_{2i} $\left[\frac{\text{degrees}}{m}\right]$ (Equation 21″) $T_1' - T_2'$ 300°	200°	100°	$q_{t_2\,max}$ $\left[\frac{kW}{m^2}\right]$ (Equation 24″) $T_1' - T_2'$ 300°	200°	100°
17	$1 \cdot 10^{-7}$	$-1.3383 \cdot 10^8$	$-8.9223 \cdot 10^7$	$-4.4611 \cdot 10^7$	$2.2751 \cdot 10^9$	$1.5167 \cdot 10^9$	$7.5839 \cdot 10^8$
	$2.1901 \cdot 10^{-7}$	$-9.0435 \cdot 10^7$	$-6.0290 \cdot 10^7$	$-3.0145 \cdot 10^7$	$1.5373 \cdot 10^9$	$1.0249 \cdot 10^9$	$5.1246 \cdot 10^8$
	$1 \cdot 10^{-6}$	$-4.2322 \cdot 10^7$	$-2.8214 \cdot 10^7$	$-1.4107 \cdot 10^7$	$7.1948 \cdot 10^8$	$4.7965 \cdot 10^8$	$2.3982 \cdot 10^8$
	$1 \cdot 10^{-5}$	$-1.3383 \cdot 10^7$	$-8.9223 \cdot 10^6$	$-4.4611 \cdot 10^6$	$2.2751 \cdot 10^8$	$1.5167 \cdot 10^8$	$7.5839 \cdot 10^7$
	$1 \cdot 10^{-4}$	$-4.2322 \cdot 10^6$	$-2.8214 \cdot 10^6$	$-1.4107 \cdot 10^6$	$7.1948 \cdot 10^7$	$4.7965 \cdot 10^7$	$2.3982 \cdot 10^7$
	$3.8633 \cdot 10^{-4}$	$-2.1532 \cdot 10^6$	$-1.4354 \cdot 10^6$	$-7.1774 \cdot 10^5$	$3.6604 \cdot 10^7$	$2.4403 \cdot 10^7$	$1.2201 \cdot 10^7$
	$1 \cdot 10^{-3}$	$-1.3383 \cdot 10^6$	$-8.9223 \cdot 10^5$	$-4.4611 \cdot 10^5$	$2.2751 \cdot 10^7$	$1.5167 \cdot 10^7$	$7.5839 \cdot 10^6$
	$2.1901 \cdot 10^{-3}$	$-9.0435 \cdot 10^5$	$-6.0290 \cdot 10^5$	$-3.0145 \cdot 10^5$	$1.5373 \cdot 10^7$	$1.0249 \cdot 10^7$	$5.1246 \cdot 10^6$

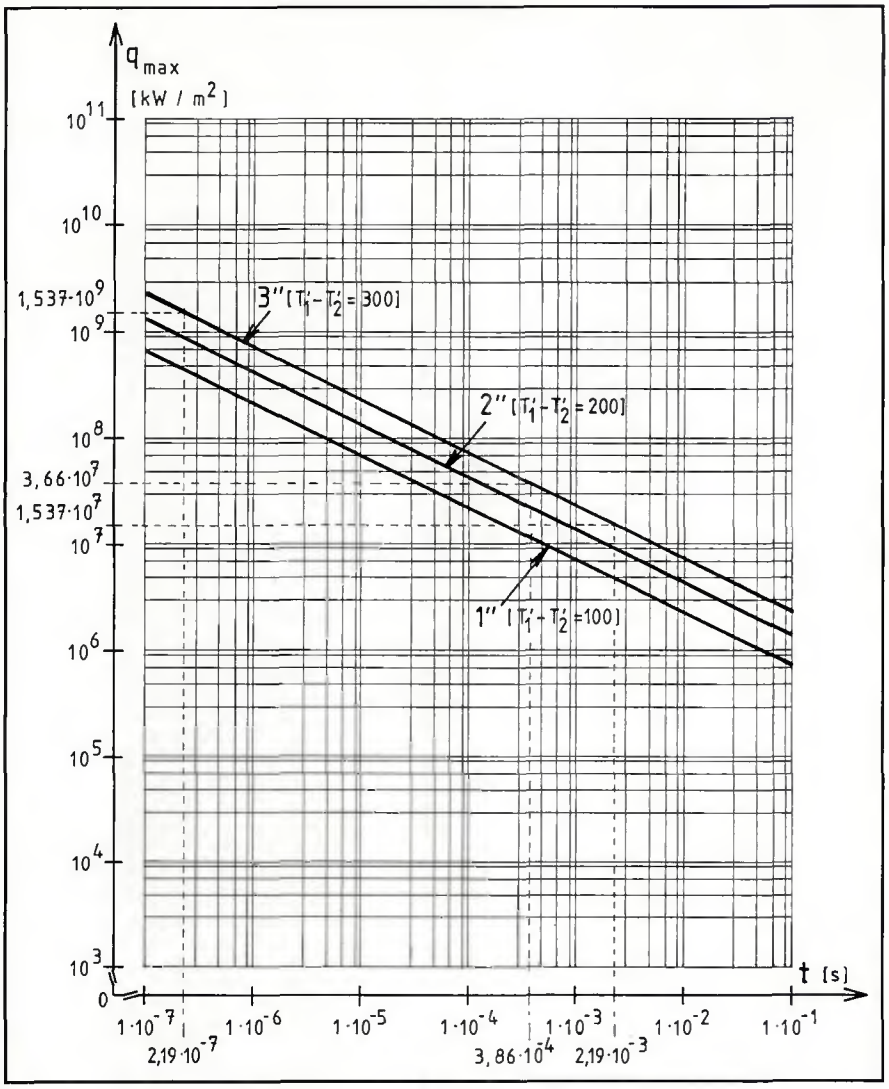

Fig. 12 – Instantaneous maximum value of the heat flux density in the surface layer of the titanium part as a function of time and the temperature difference $T'_1 - T'_2$, to which the parts have been heated before applying pressure. Temperature of the titanium part was fixed: $T'_2 = 1123$ K. Distance: $y_2 = 0^+$

mizing of the thermal effects, *viz.*, thermal spike, thermal gradient and heat flux, is beneficial to the microstructure of the boundary layer. The metallurgical aspects require shortening to the minimum high temperature influence on the joined metal. In this case, the time of DFW/TS, termed DFW/TS(S) (with thermal spike), includes two periods – Fig. 13B. The t_ι period is the interval of thermal surge heating up for the specified thickness y_ι of the boundary layer of the colder part to the contact temperature. The t_μ period is the interval for cooling down to the assumed temperature T_μ. The periods t_ι and t_μ define the dwell time of diffusion welding $t_{DFW/TS(S)}$ (with thermal spike T_s) when the dynamic variable of the contact temperature T_c is higher than T_μ, which qualifies the thermal spike duration $t_{\iota\mu}$.

One ought to emphasize that in both cases it is possible to select the heating temperatures T'_1 and T'_2 of the members so as to get a thin melted film on the surface of the colder member. It can have a beneficial effect in several cases, *e.g.*, if it is necessary to digest the oxide film.

The third variable of DFW/TS is pressure, and it can be described similarly to conventional DFW.

The time interval of each period can be readily calculated in the following terms. t_ι for the assumed distance y_ι was defined from Equations 16" and 21", yielding:

$$t_\iota = \frac{e}{2\,\alpha_2}(y_\iota)^2 \qquad (25)$$

The t_γ determines the time for DFW/TS at constant temperature, *i.e.*, as the contact temperature T_c, and is determined by way of experiment.

The t_μ was also determined by way of experimental data. The exponential equation $T_\mu = T_c \cdot \exp(-t_\mu \cdot \mu)$ (Ref. 17) can be transformed, yielding:

$$t_\mu = -\frac{\ln T_\mu - \ln T_c}{\mu} \qquad (26)$$

where: T_μ is the required temperature of the boundary layer of the joint after the cooling time t_μ; T_c is the contact temperature calculated by Equation 10; and μ is the cooling constant calculated from the characteristic of the cooling rate curve of the specified members from Equation 27:

$$\mu = -\frac{\ln T_B - \ln T_A}{t_{AB}} \qquad (27)$$

Quantities T_A, T_B and t_{AB} are measured in the initial part of this curve (Fig. 13B), and serve to calculate μ as above.

One ought to emphasize that heating of both parts to temperatures which differ from each other only by 10° also causes large thermal effects in the boundary layer, exactly in the subsurface film. As an example, when iron and titanium have been heated to 1170 and 1160 K, respectively, and pressed together, in the titanium part at the distances $y_2 = 1 \cdot 10^{-9}$ m and $y_2 = 1 \cdot 10^{-6}$ m, the instantaneous maximum values of the thermal gradient are $-3.0257 \cdot 10^9$ and $-3.0257 \cdot 10^6$ °/m, respectively, and the instantaneous maximum values of the heat flux densities are $5.144 \cdot 10^{10}$ and $5.144 \cdot 10^7$ kW/m², respectively. While two parts of titanium have been heated to 1180 and 1170 K, after having been pressed together, for the colder part, at the distances $y_2 = 1 \cdot 10^{-9}$ and $y_2 = 1 \cdot 10^{-6}$ m, the thermal gradients are $-2.4197 \cdot 10^9$ and $-2.4197 \cdot 10^6$ °/m, and the heat flux densities are $4.113 \cdot 10^{10}$ and $4.113 \cdot 10^7$ kW/m², respectively. The values were calculated on the basis of Equations 16" and 23".

Thus, with the DFW/TS process, one can get the thermal effects desired with relative ease whenever the members are heated separately.

The Equation 16 can also be used to evaluate the boundary value of the thermal gradient $G_{\iota R}$, which creates metallurgical changes at the assumed or measured distance y_{2R}. For this aim, the Equation 16 can be written as:

$$G_{\iota R} = 0.4839414\,\frac{M_1}{y_{1\iota}}(T'_1 - T'_2) \qquad (28')$$

$$G_{2\iota R} = -0.4839414\,\frac{M_2}{Y_{2\iota}}(T'_1 - T'_2) \qquad (28'')$$

Results

Diffusion Zone Structure of a Fe-Ti Joint

The influence of DFW/TS process variables on the joint structure were demonstrated on the diffusion welding equip-

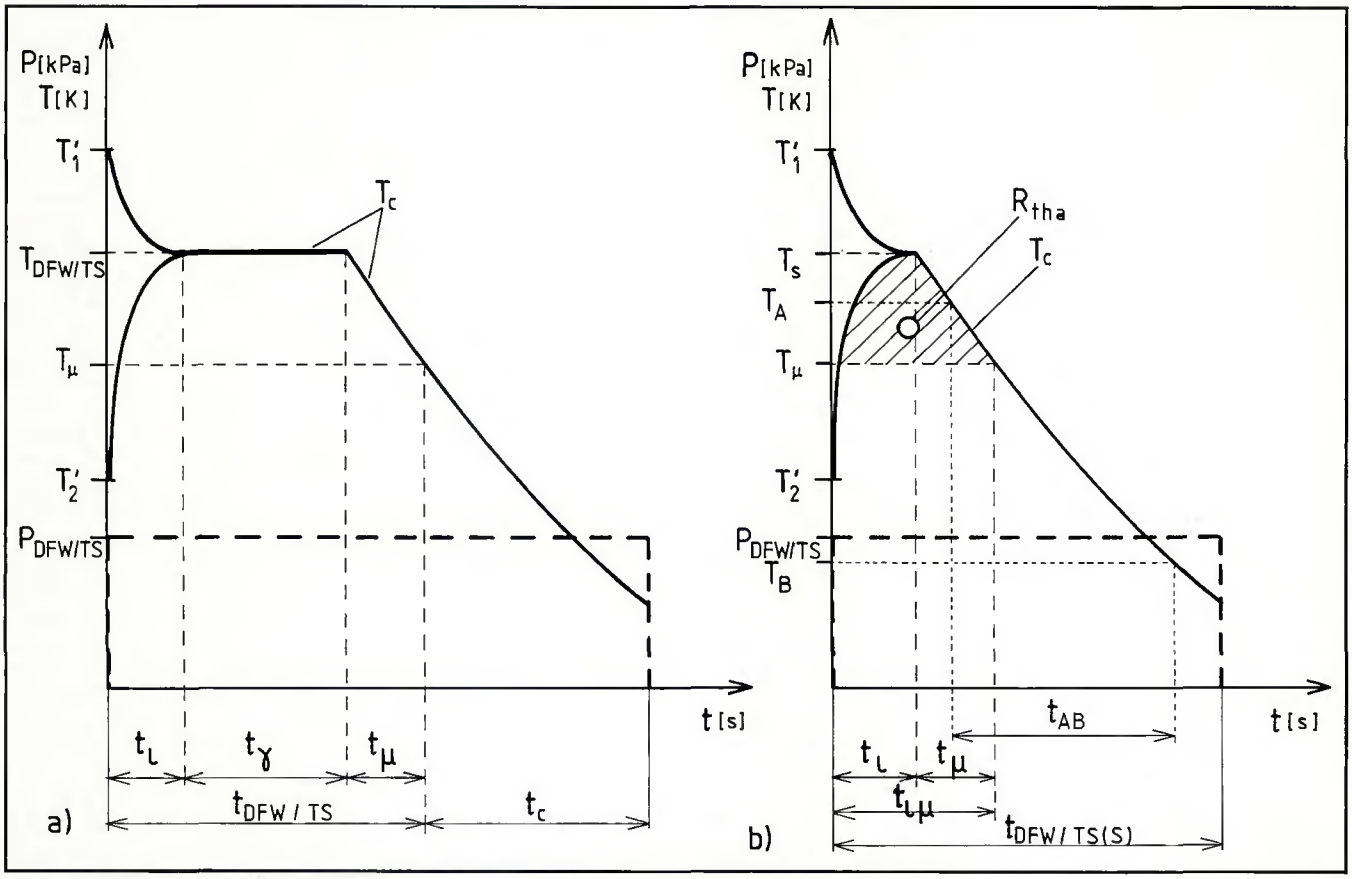

Fig. 13 — Course of contact temperature variable T_c as a time function in the process: A — When, after pressing, the continuation of the heating process for the interval of time (t_γ) brings the joint to perfection, it is termed the DFW/TS process; B — When the metallurgical aspects require shortening to the minimum high temperature influence on the joined metal, it is termed the DFW/TS(S) process, viz., DFW/TS with thermal spike T_s. R_{tha} is the range of thermal activation described by the value of thermal spike (T_s) and time of diffusion welding ($t_{DFW/TS(S)}$). Explanations for the other symbols are in the text

ment type UZD-612 (Ref. 18). The specimens of iron and titanium, 13 mm (0.51 in.) in diameter · 55 mm (2.2 in.) long, were fixed in the welding positioners W_1 and W_2 at a distance of 10 mm (0.4 in.) from each other and were heated to different temperatures T_1' and T_2' by inductors I_c composed of two parts — Fig. 14A. When the temperatures T_1' and T_2' were stabilized, the specimens were pressed to each other — Fig. 14B.

Technically, pure iron and titanium were used in the experiment. The choice of metal heated to a higher temperature T_1' and the temperature difference $T_1' - T_2'$ were made on the basis of physical and mechanical properties, and also on the diffusion coefficients of both metals (Ref. 15).

The joint structure was investigated when the variable limitations mentioned below were changed: the temperature difference $T_1' - T_2'$ from 10° to 400° and at the same time the contact temperature T_c was always higher than the transition point of $Ti_{\alpha \rightleftharpoons \beta} = 1166$ K; the time t_γ of DFW/TS at the constant temperature T_c from 600 to 0 s; the cooling rate from 2° to 40°/s, *viz.*, the time $t\mu$; the pressure per unit area from 1 to 20 MPa.

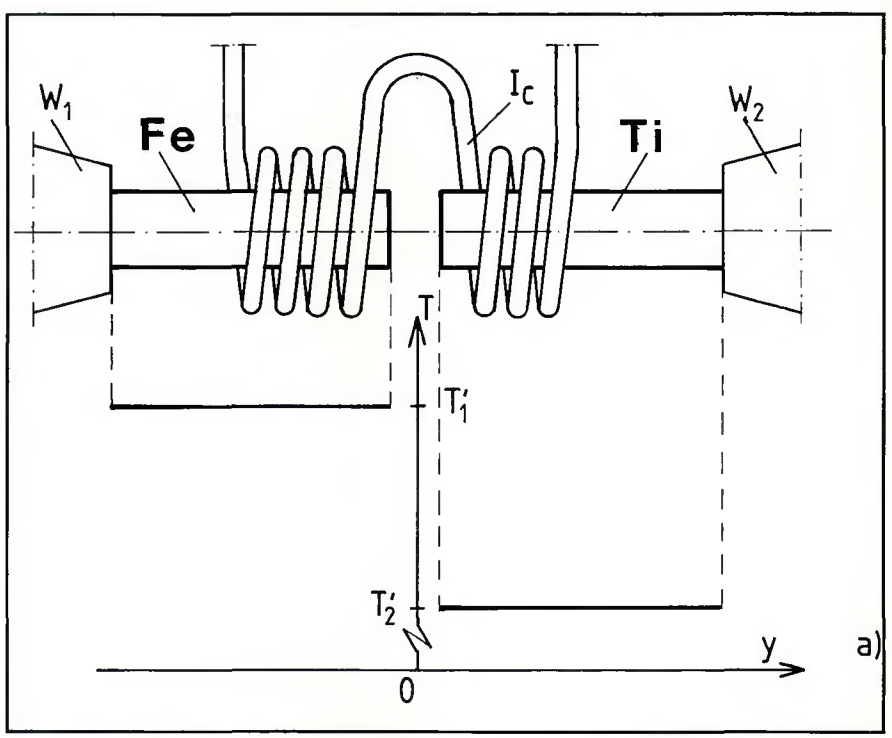

Fig. 14A — Illustration of the DFW/TS manner of heating and joining of iron and titanium specimens. Iron and titanium samples are separately heated to different temperatures T_1' and T_2', respectively

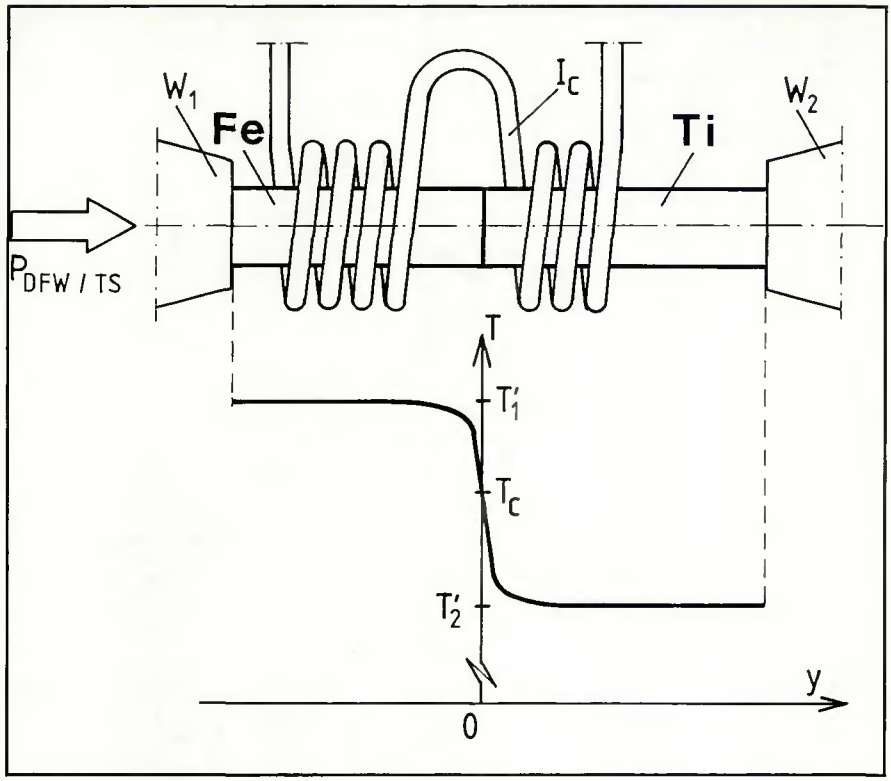

Fig. 14B – Illustration of the DFW/TS manner of heating and joining of iron and titanium specimens. Iron and titanium samples after pressing to each other with pressure $P_{DFW/TS}$; T_c is the contact temperature

The influence of process variables on the joint strength and microstructure were investigated from tensile tests, metallurgical microscopy and microhardness tests. Distribution of Fe and Ti elements in the diffusion boundary zone were analyzed with EPMA, x-ray diffraction patterns and concentration of elements by Auger analysis. The tests indicate that the best mechanical properties and most sharply defined diffusion zone resulted with the DFW/TS process when the Fe and Ti parts were heated to 1423 and 1123 K, respectively, joined with welding pressure 14 MPa, the time interval $t_\gamma = 0$ s, and the joint rapidly cooled at 30°/s. Joints made by DFW/TS(S) process had tensile strengths of 249.82 MPa, while joints made by conventional DFW had 156.20 MPa.

Figure 15 shows the Fe-Ti joint microstructure and microhardness made by DFW/TS(S) procedure. For comparison, Fig. 16 shows the results of a joint made by conventional DFW. The illustrations demonstrate the essential differences of the joints, especially of the thickness and microhardness of layers in the boundary zone.

The distribution curves of iron and titanium, and the variation in relative concentration of Fe and Ti with depth from the surface, indicate that in the joint

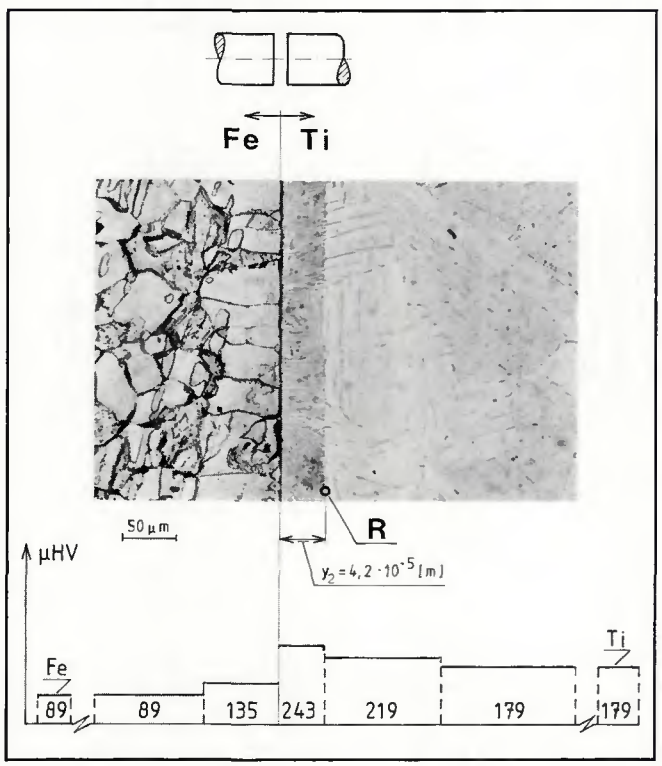

Fig. 15 – Microstructure of Fe-Ti diffusion zone joint made by DFW/TS(S) process. The variables for the DFW/TS(S) are given in Table 4. The R is the research point described in the text. The results of the microhardness test are presented below the cross-section

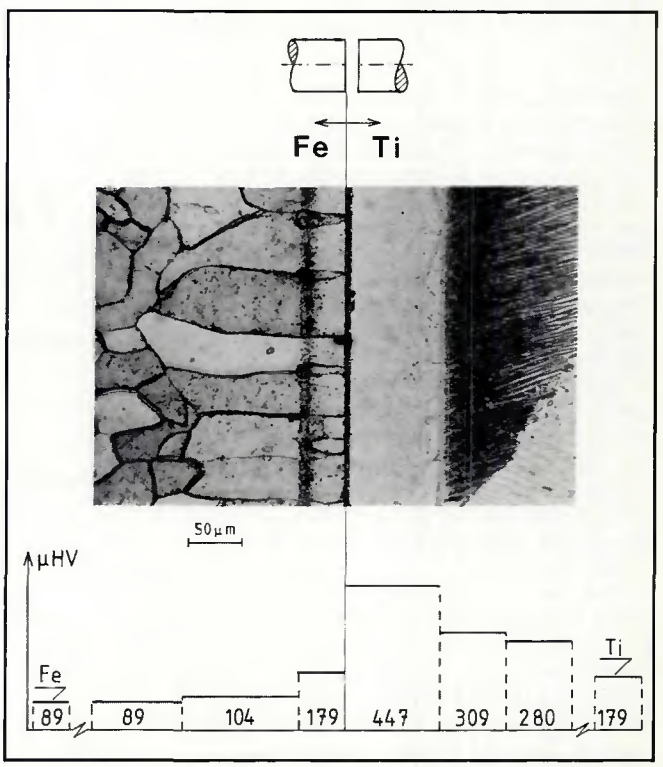

Fig. 16 – Microstructure of Fe-Ti diffusion zone joint made by the conventional DFW process. Cross-section showing the laminar structure of the boundary, diffusion zone layer. The results of the microhardness tests are presented below the cross-section. Variables for the DFW process: $T_{DFW} = 1200$ K, $t_{DFW} = 50$ min, and $P_{DFW} = 8$ MPa

made by DFW/TS or DFW/TS(S) it is possible to obtain the diffusion zone width $(2 \div 50) \cdot 10^{-6}$ m, depending on the process variable. The characteristic of the variation of distribution and the relative concentration of both elements revealed that in the diffusion zone no continuous, intermetallic compound layers were present.

The surface of the fractured joints, which have been broken at the diffusion zone, were examined with x-ray diffraction patterns. The diagrams obtained do not reveal the presence of the intermetallic compounds FeTi and Fe_2Ti. The joint made by conventional DFW was examined. In this case, the intermetallic compounds FeTi and Fe_2Ti were found in the laminar structure (Ref. 19).

From the diagrams made by the electron probe x-ray microanalyzer or by the Auger analysis, or from the photographs of the microstructure, the maximum range of diffusion in the solid state or the structural change can be read. This presents possibilities for calculating the boundary, which is minimal in absolute value, for the quantity of thermal gradient within this range of structure change. For example, at the investigated point R (Fig. 15A), at the distance $y_{2R} = 4.2 \cdot 10^{-5}$ m, at the time $t_{iR} = e \cdot (4.2 \cdot 10^{-5})^2$: $2 \cdot 6.2056 \cdot 10^{-6} = 3.8633 \cdot 10^{-4}$ s (Equation 25), the maximum absolute value of the thermal gradient is $-2\,153\,217.6$°/m (Equation 28″), and the maximum heat flux density is $q_{yR\,max} = 3.6604 \cdot 10^7$ kW/m² (Equation 23″) (Figs. 11 and 12). The above calculation can be used for the description of the thermal diffusion conditions as an effect of the thermal surge and of the thermal diffusion coefficient. It can also be used for the relations of the metallurgical process range with the boundary value of the thermal gradient G_{iR} at this point.

The value of the welding pressure was selected as a function of the heating temperature T_1' and T_2'. It was found that the range of thermal deformation in joints made by DFW/TS(S) is considerably smaller in size in comparison to joints made by conventional DFW.

Calculation of Welding Conditions for Fe-Ti Joints Made with the DFW/TS and DFW/TS(S) Processes

The ratio of the thermal effect interaction range is very small in comparison to the length of the iron and titanium specimens, and the temperature rise time of the colder member is very short. Therefore, in calculating DFW/TS and DFW/TS (S) variables, the possibility of application equations derived for the unlimited binary bar were assumed. The welding conditions for Fe-Ti joints made by DFW/TS (S) were calculated in accordance with the thermal characteristic illustrated in Fig. 13B. The calculation was simplified by the immobilization of thermal conductivities, specific heats and specific gravity values in the contact temperature T_c. Welding conditions data for the Fe-Ti joint are given in Table 4. The results of this study show that acceptance of the above assumption is reasonable.

Table 4—Welding Condition Data for Fe-Ti Joints Made by the DFW/TS(S) Procedure

Variables for DFW/TS(S)	Designation	Value	Unit of Measure	Procedure of Calculation
Temperature of iron member	T_1'	1423	K	Assumption in accordance with Fig. 5
Temperature of titanium member	T_2'	1123	K	Assumption in accordance with Fig. 5
Temperature difference	$T_1' - T_2'$	300°	degrees	
Contact temperature	T_c	1310	K	Equation 10
Transfer coefficient	M_2	0.6229069	–	Equation 9″
Distance y_{2R} from the research point R	y_{2R}	$4.2 \cdot 10^{-5}$	m	measured or assumed
Time of heat up of the specified thickness y_{2R} of the boundary layer	t_{iR}	$3.8633 \cdot 10^{-4}$	s	Equation 25
Instantaneous boundary value of the thermal gradient in the investigated point R at distances y_{2R} from the connected surfaces	G_{2R}	$2.153217 \cdot 10^6$	$\frac{\text{degrees}}{\text{m}}$	Equation 28
Instantaneous value of the heat flux density at the investigated point R	$q_{y_2\,max}$	$3.6604 \cdot 10^7$	$\frac{\text{kW}}{\text{m}^2}$	Equation 23″
	$q_{t_2\,max}$	$3.6604 \cdot 10^7$	$\frac{\text{kW}}{\text{m}^2}$	Equation 24″
Temperature	T_A	1400	K	measured (Fig. 13B)
Temperature	T_B	1114	K	measured (Fig. 13B)
Time of cooling down	t_{AB}	10	s	measured (Fig. 13B)
Cooling constant	μ	0.0228515	$\frac{1}{\text{s}}$	Equation 27
Interval of cooling down of Fe-Ti joint to the assumed temperature $T_\mu = 1166$ K	t_μ	5.09586	s	Equation 26
Thermal spike duration	$t_{i\mu}$	5.10711	s	$t_i + t_\mu$
The end temperature for DFW/TS	T_μ	1166	K	Assumption in accordance with Fig. 5
Welding pressure	$P_{DFW/TS(S)}$	14	MPa	Determined by experiments

Conclusions

The results obtained from evaluations of thermal effects, thermal spike, thermal gradient and heat flux density, as well as investigations of the diffusion zone structure of Fe-Ti joints made by DFW/TS(S), enable the following conclusions to be made:

1. Introduction to diffusion welding of the procedure consisting of heating the separate members to different temperatures generates, after pressing to each other, a thermal surge in the boundary layer of the joint.

2. Thermal surge characteristic investigations, made on the basis of a mathematical model, showed that in the boundary layer of the unlimited bar, composed of iron and titanium parts, large thermal effects, *viz.*, thermal spike, thermal gradient and heat flux, come into existence.

3. The following have an essential influence on the values and dynamics of the thermal variations: the temperature level and temperature difference of the members, and the physical properties at high temperatures of the metals which have been joined, *viz.*, thermal conductivity, specific heat and specific gravity.

4. The maximum momentary heat flux density generated in the boundary layer by DFW/TS procedure attains a value similar to the analogical, but constant in time, values given by the laser or electron beam equipment.

5. The thermal spike, thermal gradient and heat flux generated by DFW/TS procedure provoke thermal diffusion on the boundary layer.

6. Experience with the introduction of the thermal spike to diffusion welding and mathematical formulation of DFW/TS variables enables this procedure to be used in practice and forms the basis for further investigations on the structure and quality of welds made by DFW/TS.

Appendix

Symbols Used

1 and 2	symbols designating the hotter and colder part, respectively, and in later calculations, the iron and titanium members, respectively
0	contact surfaces for both parts (members) and the moment of pressing of the parts to each other
y	distance from contact surfaces, where $y_1 \leq 0$ and $y_2 \geq 0$, m
y_ι	specified thickness of the boundary layers of the colder part (Equation 25), m
t	time measured from the moment pressure is applied to both members, s
t_{ex}	time defined for the extreme value in calculations, s
t_ι	time of heating up of the specified thickness y_ι of the boundary layer of the colder member to contact temperature T_c by the thermal surge (Equation 25), s
t_γ	time of diffusion welding at constant temperature T_c, s
t_μ	cooling time of the joint from one temperature to the other, specific for members and equipment. In these calculations it describes the cooling time of members from T_c to T_μ (Equation 26), s
$t_{\iota\mu}$	time of thermal spike duration, s
$t_{DFW/TS}$	time of diffusion welding with the thermal surge; contains the periods t_ι, t_γ, t_μ
$t_{DFW/TS(S)}$	time of diffusion welding with the thermal surge and thermal spike; contains the periods t_ι, t_μ
T'	temperature of the members before pressing, K
T_c	contact temperature of two members (Equation 10), K
T_s	thermal spike value in DFW/TS(S) is equal to the maximum momentary value of contact temperature T_c (Equation 10), K
T	temperature of the joint at the variable distance y and time t, K
T_{ex}	extreme value of temperature in the calculations, K
T_μ	optional temperature which defines the end of the diffusion process, K
T_A, T_B	experimental quantities from the cooling curve (Equation 27), K
DFW	diffusion welding as defined in AWS A3.0-80, *Standard Welding Terms and Definitions*
DFW/TS	diffusion welding with thermal surge
DFW/TS (S)	diffusion welding with thermal surge and thermal spike
M	transfer coefficient as the dimensionless quantity (Equation 9)
$G_{\iota R}$	instantaneous boundary value of the thermal gradient at the measured distance y_{2R} (Equation 28)
$q_{y\ max}$	heat flux density in distance function (Equation 23), kW/m^2
$q_{t\ max}$	heat flux density as a time function (Equation 24), kW/m^2
λ	thermal conductivity, W/m · K
c_p	specific heat, J/kg · K
g	specific gravities, kg/m^3
α	thermal conductance which occurs in Equation 4 for heat conduction, m^2/s
τ	slack variable for time interpretation (Equations 6, 7)
θ	optional function determined later from boundary conditions (Equations 6, 7)
μ	cooling constant described in Equations 26 and 27
$\frac{\partial T}{\partial y}(y,t)$	thermal gradient value at point y and time t, °/m
$\frac{\partial T_{ex}}{\partial y}(y,t)$	extreme thermal gradient value at point y and time t_{ex}, °/m

Acknowledgments

The author wishes to express his appreciation to H. B. Müller and R. Welzel for their help in the numerical calculations, and J. Ploch for his help in mathematical modelling of the problem. This work was supported by the Jülich Nuclear Research Center—KFA and the Technical University of Warsaw.

References

1. Pietrov, G. L., Tumasiev, A. S. 1977. *Theory of Welding Processes*. p. 392, High School, Moscow, USSR.

2. Enjo, T., Ikeuchi, K., Akikawa, N. 1981. Effect of oxide film on the early process of diffusion welding. *Transactions of JWRI* 10(2):45-53.

3. Enjo, T., Ikeuchi, K., Akikawa, N. 1979. Diffusion welding of copper to aluminum. *Transactions of JWRI* 8(1):77-84.

4. Lundin, C. D. 1982. Dissimilar metal welds—transition joints literature review. *Welding Journal* 61(2):58-s to 63-s.

5. Enjo, T., Ikeuchi, K., Akikawa, N., Ito, M. 1980. Effect of superplasticity on the diffusion welding of Ti-6Al-4V alloys. *IIW Doc. I-GT.dif.* 06-80:1-7.

6. Bryant, W. A. 1975. A method for specifying hot isostatic pressure welding parameters. *Welding Journal* 54(12):433-s to 435-s.

7. Kramer, I. R., Burrows, C. F. Diffusion bonding. USA Patent No. 3256598.

8. Godziemba-Maliszewski, J. A manner of diffusion welding. Polish Patent No. 106167.

9. Godziemba-Maliszewski, J. A manner and device for diffusion welding. Polish Patent No. 101239.

10. Kazakov, N. F. 1976. *Diffusion Welding of Materials*. p. 312, Mashinostroenije, Moscow, USSR.

11. Christ, H. J., Ilschner, B. 1983. Calculation of diffusion processes in the presence of a temperature gradient. *Scripta Metallurgica* 17:631-634.

12. Buda, M. J. 1980. Studies on effects of a temperature gradient migration of the components in a solid state system. Appendix to Military Technical College, Bulletin No. 1.

13. Godziemba-Maliszewski, J. A manner of thermomechanical diffusion welding. Polish Patent No. P.240726.

14. ASM Handbook Committee. 1973. *Metals Handbook*, Vol. 8, American Society for Metals, Metals Park, Ohio.

15. *Smithells Metals Reference Book*, Sixth Edition. 1983. Butterworths, London, England.

16. Goldsmith, A., Waterman, T. E., Hirschhorn, H. J. 1961. *Handbook of Thermophysical Properties of Solid Materials*. Pergamon Press, New York, N.Y.

17. Rykalin, N. N. 1957. *Berechnung der Wärmevorgänge beim Schweissen*. p. 326, VEB Verlag Technik, Berlin, Germany.

18. Godziemba-Maliszewski, J. 1983. Vacuum diffusion welding system. *Schweisstechnik* 33(9):424-426.

19. Godziemba-Maliszewski, J., Fiett, M. 1985. Effects of the manner of heating on the process of diffusion welding on the structure of Fe-Ti joint. *Archiwum Hutnictwa* 30(2):111-134.

20. Kubaschewski, O. 1982. *Iron-Binary Phase Diagrams*. p. 186. Verlag Stahleisen m.b.H, Düsseldorf, Germany.

21. Arata, Y., Ohmori, A., Fu Cai, H. 1983. Studies on vacuum brazing—report II. *Transactions of JWRI* 12(1):27-34.

An Invitation to Participate in POSTER SESSIONS at the 69th Annual AWS Convention New Orleans, Louisiana, April 17–22, 1988

. . . is being extended to researchers, educators, students, welders, distributors, customers, artists, and others whose technical accomplishments benefitting the welding community lend themselves to brief, graphic presentation for close, first-hand examination by interested individuals, rather than to verbal presentation before a large audience. For many, Poster Sessions will be an ideal format to present:

- results that are best communicated visually.
- new techniques or procedures that are best discussed in detail with interested viewers.
- brief reports on work in progress.
- results calling for close study of photomicrographs or other illustrative materials.

Rules

1. Complete the Poster Session Application on the other side of this announcement and mail it with a 100- to 150-word description (*i.e.,* abstract) of your Poster Session topic by November 1, 1987, to Secretary, Technical Papers Committee, American Welding Society, 550 N. W. LeJeune Rd., P. O. Box 351040, Miami, FL 33135.

2. If you are notified during December 1987 that your proposed Poster Session topic has been accepted, you should:

   - mount your material on either 22-in.-high × 28-in.-wide or 44-in.-high × 28-in.-wide (maximum size) poster board, or prepare your material so that it can be mounted for you on one of those sizes of poster board.
   - plan to use type that is large enough that it can be read from 3 to 6 ft away.
   - be sure not to superimpose sheets of text or illustrations on top of each other.
   - mail or ship your poster (or poster material) so that it reaches AWS by February 29, 1988. All posters (or poster material) become the property of AWS and will not be returned. (For poster material to be mounted for you, include a sketch, or layout, keyed to your material to show how your material should be mounted.)
   - indicate below whether you will or will not be present in New Orleans for discussion of your poster. Attendance in New Orleans is not mandatory.

Yes, I will be present _____ No, I will not be present _____

IMPORTANT: Only material that does not exceed the space available on one 44- × 28-in. poster board will be acceptable.

POSTER SESSION APPLICATION

for

69th Annual AWS Convention

New Orleans, Louisiana, April 17–22, 1988

Fill in information called for below and mail with 100- to 150-word abstract by November 1, 1987, to:

Secretary
Technical Papers Committee
American Welding Society
P. O. Box 351040
Miami, FL 33135

Date Mailed .....

Poster Author's Name ..... Check how addressed: Mr. ☐ Ms. ☐

Title or Position ..... Dr. ☐ Other .....

Company or Organization .....

Mailing Address .....

City ..... State ..... Zip ..... Telephone: Area ..... Number .....

If there are to be joint authors, give name(s) of other author(s)

Name .....
Address .....
Name .....
Address .....

TOPIC TITLE OR DESCRIPTION: _____

Abstract

The 100- to 150-word abstract should include information regarding:

- overall significance of the poster for viewers.
- the newness or originality of the poster materials.
- welding conditions, *i.e.*, process, current, voltage, welding speed, base and filler metal, and (when used) shielding gas flow rates and composition.
- what your illustrations (if any) show.
- the more important points that the poster stresses.
- where relevant, the economic effects of the work described by the poster.

Poster Presentation in New Orleans

The presence of a personal representative in New Orleans is not mandatory. However, if a representative is to be present, that person should plan to be present by the poster at a time when the formal oral Technical Sessions are not being held – for example, for at least one hour between 12 noon and 1:30 p.m. April 18 or one hour between 12 noon and 2 p.m. April 19–21. Please indicate the times you would be at your poster if your Poster Session topic is selected:

April 18 _____ April 19 _____ April 20 _____ April 21 _____

Return to AWS Headquarters by November 1, 1987, with 100- to 150-word abstract to ensure consideration.

_____
Poster Author's Signature